SOL-GEL PROCESSING OF SILVER-DOPED SILICA AND ASSESSMENT OF ITS STRUCTURAL AND ANTIMICROBIAL PROPERTIES

A THESIS SUBMITTED TO
THE GRADUATE SCHOOL OF NATURAL AND APPLIED SCIENCES
OF
MIDDLE EAST TECHNICAL UNIVERSITY

BY

BETÜL AKKÖPRÜ-AKGÜN

IN PARTIAL FULFILLMENT OF THE REQUIREMENTS
FOR
THE DEGREE OF MASTER OF SCIENCE
IN
METALLURGICAL AND MATERIALS ENGINEERING

SEPTEMBER 2015

.

Approval of the thesis:

SOL-GEL PROCESSING OF SILVER-DOPED SILICA AND ASSESSMENT OF ITS STRUCTURAL AND ANTIMICROBIAL PROPERTIES

submitted by **BETÜL AKKÖPRÜ-AKGÜN** in partial fulfillment of the requirements for the degree of **Master of Science in Metalurgical and Materials Science and Engineering Department, Middle East Technical University** by,

Prof. Dr. Gülbin Dural Ünver _____
Dean, Graduate School of **Natural and Applied Sciences**

Prof. Dr. C. Hakan Gür _____
Head of Department, **Metallurgical and Materials Engineering**

Prof. Dr. Caner Durucan _____
Supervisor, **Metallurgical and Materials Engineering Dept., METU**

Examining Committee Members:

Prof. Dr. Tayfur Öztürk _____
Metallurgical and Materials Engineering Dept, METU

Prof. Dr. Caner Durucan _____
Metallurgical and Materials Engineering Dept, METU

Prof. Dr. Kadri Aydınol _____
Metallurgical and Materials Engineering Dept, METU

Assoc. Prof. Dr. Burcu Akata Kurç _____
Micro and Nanotechnology Dept., METU

Assist. Prof. Dr. İlkay Saltoğlu Kalay _____
Materials Science and Engineering Dept., Çankaya University

Date: *11.09.2015*

I hereby declare that all information in this document has been obtained and presented in accordance with academic rules and ethical conduct. I also declare that, as required by these rules and conduct, I have fully cited and referenced all material and results that are not original to this work.

Name, Last name: Betül Akköprü-Akgün

Signature

ABSTRACT

SOL-GEL PROCESSING OF SILVER-DOPED SILICA AND ASSESSMENT OF ITS STRUCTURAL AND ANTIMICROBIAL PROPERTIES

AKKÖPRÜ-AKGÜN, Betül

Master of Science, Department of Metallurgical and Materials Engineering

Supervisor: Prof. Dr. Caner DURUCAN

September 2015, 74 pages

Sol-gel processing routes for development of silver biocide-doped antibacterial silicate based coatings and powders were established and structural properties defining the antibacterial activity and long term durability were determined. During the first phase of this study, silver-doped silica based powders have been synthesized by hydrolysis and condensation of tetraethyl orthosilicate (TEOS, $Si(OC_2H_5)_4$) in the presence of a silver nitrate ($AgNO_3$) solution. The effects of modifications in sol-gel chemistry -acid catalysis and acid/base catalysis- and subsequent heat treatments on silica microstructure and on silver particles size were investigated. The acid-catalyzed sol-gels formed a microporous silica network whereas the two-step catalyzed silica exhibited a mesoporous structure. It was found that mesoporous structure leads to formation of bigger silver particles and promotes crystallization of silica network upon calcination and improving the antibacterial performance. In the following phase, silver nanoparticle containing silica coatings on soda-lime glass were prepared by the sol–gel process. The

effect of thermal densification treatment at different temperatures in the range of 100–700ºC on microstructure and antibacterial properties of the coatings were examined. The mechanisms for formation and distribution of silver nanoparticles in the silica matrix with respect to the calcination temperature were discussed, and the correlation between the microstructural properties and antibacterial activity was described. The investigations revealed that silver nanoparticles were mainly in the metallic state during thermal treatments and silver accumulated on the surface diffuse into glass substrate at higher calcination temperatures. A high level of antibacterial activity was observed for the coatings calcined at 300ºC or lower temperatures allowing accommodation of silver on the surface of the coating. Silver diffusion into bulk via ion-exchange with sodium and calcium ions from glass substrate during calcination at higher temperatures (500 or 700ºC) resulted in apparent degradation in the antibacterial activity.

Keywords: sol-gel, silica, silver nanoparticle, antibacterial

ÖZ

SOL-JEL YÖNTEMİYLE GÜMÜŞ-AŞILANMIŞ SİLİKAT ESASLI MALZEMELERİN GELİŞTİRİLMESİ VE YAPISAL VE ANTİBAKTERİYEL ÖZELLİKLERİNİN KARAKTERİZASYONU

AKKÖPRÜ-AKGÜN, Betül

Yüksek Lisans, Metalurji ve Malzeme Mühendisliği Bölümü

Tez Yöneticisi: Prof. Dr. Caner DURUCAN

Eylül 2015, 74 sayfa

Gümüş biyosit taşıyan silika esaslı antibakteriyel malzemelerin kaplama ve toz formunda sol-jel metodu ile üretim süreçleri belirlenmiş ve bu sistemlerde antibakteriyel aktiviteyi ve dayanımı belirleyen malzeme özellikleri tanımlanmıştır. Projenin ilk aşamasında gümüş aşılanmış silika esaslı tozlar tetraetil ortosilikat ve gümüş nitrat solüsyonlarının hidroliz ve yoğunlasma reaksiyonları sonucu elde edilmistir. Sol-jel kimyasında yapılan değişimlerin - asit katalizleme, asit/baz katalizleme- ve takip eden ısıl işlemlerin silika mikroyapısına ve gümüş parçacık boyutuna olan etkileri incelenmiştir. Asit katalizleme metodu ile elde edilen tozlar mikroporoz bir yapı gösterirken, asit-baz katalizleme metodu ile üretilen tozların, daha büyük gözenekli (mesoporoz) bir yapı gösterdiği bulunmuştur. Mesoporoz yapının daha büyük gümüş parçacık oluşumuna neden olarak, silika matrisin kristalleşmesini kolaylaştırdığı ve antibakteriyel performansı arttırdığı bulunmuştur. Takip eden çalışmalarda toz üretimi

esnasında kullanılan sol formülasyonlari kullanılarak gümüş aşılanmış cam üstü kaplamalar hazırlanmıştır. Kaplama sonrası uygulanan ısıl işlem sıcaklığının (100-700 ºC) yapısal ve antibakteriyel özelliklere olan etkisi incelenmiştir. Gümüş nanoparçacıkların silika matriks içindeki oluşum mekanizması açıklanmıştır ve yapısal ve antibakteriyel performans özellikler arasındaki ilişki tanımlanmıştır. Göreceli olarak düşük sıcaklıklarda gerçekleştirilen ısıl işlem sonucu gümüşün metalik formda kaplama yüzeyine yakın bulunduğu gözlemlenmiştir. Gümüş nanoparçacıkların yüzeye yakın bulunduğu bu kaplamaların yüksek antibakteriyel özellik gösterdiği bulunmuştur. Kalsinasyon sıcaklığının 500 ºC ve üzerine artışı ile birlikte yüzeye yakın yerlerde bulunan gümüş parçacıkların cam altlığa difuz ettiği ve buna bağlı olarak antibakteriyel performansın azaldığı gözlemlenmiştir.

Anahtar kelimeler: sol-jel, silika, gümüş nano parçacıkları, antibakteriyel

ACKNOWLEDGEMENTS

I would first like to acknowledge the support and guidance, which I have received over the past years from my advisor Dr. Caner Durucan. I would also like to like to thank my committee, Drs Öztürk, Aydınol, Akata-Kurç, and Saltoğlu-Kalay.

Very special thanks to my collaborators Dr. Mellott, Dr. Towler, and Dr. Wren for always being supportive during my stay at Alfred University. Your insightful discussions improved the quality of this research.

And finally, I am grateful for the love and support of my parents, my husband and my little one. Your support and love kept me going throughout this process.

TABLE OF CONTENTS

LIST OF TABLES

LIST OF FIGURES

CHAPTER 1

GENERAL INTRODUCTION and BACKGROUND INFORMATION

1.1 General introduction and rationale of the thesis

There is an urgent need for development of new functional materials that prevent the survival and growth of microorganisms due to spread of antibiotic-resistant infections. Among a variety of biocides, silver nanoparticles have been proven to be the most effective in preventing proliferation of broad-spectrum microorganisms, including gram-negative [1], gram-positive [2] bacteria, viruses [3], and fungi [4]. They also exhibit high biocompatibility, high thermal stability, and non-toxicity to human cells, which results in increasing use of silver nanoparticles as an antibacterial material in biomedical applications, water and air purifications, textiles, and household products [5].

Up to now, different models have been suggested in the literature to explain the antimicrobial mechanism of silver. Although a great number of studies has been attempted to explore antibacterial effect of silver nanoparticles, a relatively modest number of studies have been conducted to understand antibacterial mechanism of silver. It is commonly believed that the antibacterial activity of silver starts with release of Ag^+ as a result of interaction of silver nanoparticles with moisture of bacteria cell. Then there is a generation of reactive oxygen species, which can easily attached to vital enzyme groups on bacteria cell wall [6]. When, these functional enzymes are inactivated, bacteria can no longer perform survival activies, like respiration and nutrition. This

damages the bacteria cells and eventually leads to termination of celluler activities and cell death [7-8].

Since the antibacterial activity of silver is strongly dependent on release of silver ions, reactivity and dissolution of silver are significant parameters that influence formation of ROS and final antibacterial property. It has been found that surface reactivity and dissolution of silver particles are greatly affected by size and shape of silver nanoparticles. Smaller silver nanoparticles provide higher surface area and thus larger contact area for interaction with bacteria. This enhances release of higher concentration of silver ions to inactivate the vital enzyme groups and destroy the bacteria cell [9-10]. Additionally, the shape of silver nanoparticles also influences antibacterial activity. It was shown that silver particles having triangular and rod shapes exhibit higher bactericidal activity compared to their spherical counterparts because of high atomic density plane {111} that promotes the interaction with cell membrane [11]. It has been also suggested that {111} hexagonal high energy defect sites in {111} fcc facets act as a preferential sites for interaction with bacteria cell wall and thus enhancing antibacterial activity [11].

Although rod or/and triangular shaped nanosized silver particle is desired to attain high bactericidal activity, chemical and physical stability of silver nanoparticles are challenging tasks due to their affinity to get flocculated and oxidized under ambient conditions. Silver nanoparticles are thermodynamically unstable and thus can easily form agglomerates to decrease their surface energy thus becoming more stable. Agglomeration of silver nanoparticles reduces the effective surface area, which is available for interaction with bacteria cell, which in turn weakens the resultant bactericidal activity [12]. Moreover, silver nanoparticles might get oxidized under ambient conditions. These newly formed oxide compounds of silver can be easily dissolved in a short time, which in turn drastically reduces the long-term bactericidal activity [13].

Two overcome two aforementioned problems; oxidation and agglomeration of silver

nanoparticles, silver particles are embedded into organic or inorganic matrices, such as zirconia [14], titania [15], zeolite [16], silica [17], and polysterene [18]. These organic and inorganic matrices also provides homogenous dispersion of silver particles throughout the matrix, promoting long lasting bactericidal activity due to slow release of silver ions in a long time. Among different matrices, inorganic silica matrix acts as most convenient carrier for incorporating silver nanoparticles because of its high physical, mechanical, thermal and chemical stability. In this respect, silver embedded silica powders and coatings have been developed and commonly used in applications, such as coatings of biomedical implants and medical devices, water filters, textiles, and glass surfaces. Different methods have been suggested in the literature to incorporate silver into silica matrix, including sol-gel [19], sputtering [20], ion implantation [21], and ion exchange [22]. Among these distinct methods, sol-gel technique enables mixing at an atomic level, which provides control over chemical and physical state of silver and silica matrix and particle size and distribution of silver. This helps understanding essential physical and microstructural properties of Ag-SiO_2 system to attain long-lasting antibacterial activity. The chemical state and particle size of silver as well as microstructure and crystal phase of silica matrix, which greatly affect the long-lasting bactericidal property can be controlled by modification of initial sol-gel processing parameters, such as nature of catalysis, silver source, silicon alkoxide type, heat treatment temperature and atmosphere, TEOS:H_2O molar ratio.

The main objective of the proposed work is to establish processing routes for the development of a durable antibacterial silicate based powders and coatings doped with a natural biocide-silver- by sol-gel technique. The produced material will be effective against generic bacteria such as S*taphylococcus Aureus* ve *Escherichia Coli*. The study will mainly focus on the synthesis of silver doped silica powders and coating on glass surfaces. In the first phase of the study, sol-gel processing parameters that enable control of the chemical state and distribution of silver in silica matrix and the modification of surface physical properties will be determined using experimental methods and analytical material characterization techniques. In the second phase of the thesis, a variety of sol-gel coatings with tailored properties will then be tested for their

antibacterial performance and durability under chemical and environmental conditions simulating their use in service. The target values for the antibacterial materials that are going to produce in this study can be summarized like: (a) highly biocidal long after its application to the surface, (b) non toxic, causticor corrosive, (c) colorless, chemically durable which release silver ion for a long period of time.

1.2 Background information and literature review

The synthesis and processing of antibacterial powders and coatings, which prevent the adhesion and growth of the bacteria on the surfaces, has attracted great attention due to increasing hygiene concerns. There are several approaches and systems, which can be used for antibacterial applications.

1.2.1 Systems which minimize physical contact of bacteria with surfaces: Organic coatings such as polyethylene glycol (PEG) [23] or fluoro hydrophobic surfaces are belonging to this group of antibacterial materials. They only minimize the physical contact of bacteria with surfaces and bacteria are still alive after this interaction. These organic surfaces suffer from structural instability against environmental factors, such as UV during long-term services. Therefore, they are used in limited application fields [23].

1.2.2 Coatings which destroy bacteria by contact: This kind of coatings includes specially synthesized polymers with long and stiff hydrocarbon arms, which destroy the bacterial cell walls as a molecular knife. Poly (4-vinylpyridne) with long alkali group can be considered as an example [24-25]. They only have effect on airbone bacteria and do not show antibacterial properties when coated on metal and polymer surfaces [25].

1.2.3 Coatings which includes active biocides: This kind of systems provides releasing of active biocides, which is responsible from antibacterial property for a long term. In the literature, antibiotics [26], chlorine [27], iodine [28] have been suggested as examples. In general, biocides destroy wall of the bacteria cell and cause changes in

enzymatic activities controlling nutrition and respiration. However, these systems are insufficient due to the incompatibility of the active biocides with the human tissues. In addition, bacteria can develop a natural immune response against the antibiotics and thus, antibiotic biocides lose their antibacterial effect on bacteria with time [26].

Silver as an antibacecterial material

As an alternative, silver doped silica based materials are good candidates for antibacterial applications considering their broad-spectrum biocidal activity, relatively low cost, high biocompatibility and nontoxicity properties. In addition, silver does not foster the development of resistant organism and continues to be highly biocidal long after its application to the surface.

Antibacterial property of silver comes from dissociation of silver ion (Ag^+) from silica matrix when exposed to bacteria colonies. Antibacterial activity of silver is attained by the interaction of released Ag^+ ion with thiol (sulphydryl, –SH) groups located on the cell wall. After the interaction, S-Ag complexes form on bacteria cell wall, preventing replication and respiration of bacteria. The release of Ag ion is one of the most important factors determining antibacterial performance. The dissolution of silver takes place through redox reaction involving dissolved oxygen and proton [29]:

$$4Ag + O_2 + 2H_2O = 4Ag^+ + 4OH^- \quad [1]$$

The release rate of silver ion determines how fast the silver nanoparticles is consumed which in turn define lifetime of antibacterial material. For most of the application, chemically durable antibacterial materials releasing ion for a long period of time is desired. Thus, silver particles were doped into silica matrix in this study. The silver ion release is influenced by physical, chemical and structural properties of $Ag\text{-}SiO_2$ systems. These parameters are particle size and shape of silver, chemical state of silver as well as morphology of silica [29].

1.2.4 Silver doped silica based antibacterial materials

Metallic silver formation mechanism

Silver nanoparticles can be introduced into silica matrix by dissolution of silver source (silver nitrate) in silica sol. Then, reduction of silver ions to metallic silver particles is realized by (1) heat treatment in air and/or reducing gas, (2) UV-exposure. Although the physical mechanism behind metallic silver formation is still uncertain, some researchers proposed that non-bridging Si–O groups converts into the Si–O–Ag by a cation exchange process as follows [30] :

$$\equiv \mathrm{Si-OH} + \mathrm{Ag^{+}} \rightarrow \equiv \mathrm{Si-O-Ag} + \mathrm{H^{+}}. \quad [2]$$

It is widely accepted that water and organic compound are removed from silica network during densification of the gels. Subsequent heat reatments enhance crystallization of the amorphous SiO_2 sol–gel. It was found that annealing temperature greatly affects the reduction of Ag^+ ions [31].

Calcination treatments for silver-doped silica based coatings can be done under oxidative atmosphere (air) or, reductive atmosphere (H_2, N_2 or Ar). Heating medium is important to control the reduction of silver ions to metallic silver colloids. It was observed that silver mostly remained in ionic state (Ag^+) and no silver nanoparticles formed under oxidizing atmosphere [32]. On the other hand, the samples annealed under N_2–H_2 showed a small amount of metallic silver formation. Once silver colloids generated, heat treatments at high temperatures (600 °C) results in rapid growth of preformed silver particles [33].

Addition of modifiers, such as arsenic oxide also facilitates reduction of silver ions to metallic silver nanoparticles. Villegas et al. investigated the effect of arsenic oxide addition on metallic silver formation for films heat treated under both oxidative and reductive environments. It was found that, the amount of arsenic oxide required for metallic silver formation is less under reductive atmosphere compared to oxidative

atmosphere [34]. This was attributed to partial densification of gel to silica network under air since Ag^+ ions, which are coordinated by oxygen in polysiloxane bonds, act as modifier ions [34].

Surface chemical composition of substrate also has an important affect on ionic silver reduction process. Suyal et al. studied the effect of tin-rich substrate on metallic silver nanoparticle formation. It was found that, formation of the silver colloids was greatly affected by surface of the float glass. While formation of metallic silver was observed on tin rich surface, silver mostly remained as in ionic state on tin poor surface. The dependence of metallic silver formation on substrate was attributed to the oxidization of Sn^{2+} to Sn^{4+} on glass surface, which enables silver ions to reduce to metallic silver particles [35].

Oxidization of metallic silver nanoparticles

Metallic silver colloids get oxidized upon heat treatment at moderate temperatures around 400-500°C that can be identified by a blueshift of surface plasmon resonance peak of silver in UV-vis spectra or color change in the color of the films. When Ag^+ ions form Ag_xO_y compounds, the coating color becomes transparent. However this bleaching effect is reversible [36]. When they are exposed to light or heat-treatment at temperatures higher than 600°C, the color turns back into yellowish and becomes stable since silver metal particles completely embedded in SiO_2 matrix [36-38].

Diffusion of silver ions through substrate

One of the problems related to silver doped silica coatings is diffusion of silver through glass substrate during heat treatment. Silver in ionic state, Ag^+, can easily go through ionic exchange process with mobile ions, such as Na^+ and Ca^{2+} in glass. Garcia et al. found that ionic exchange process between Ag^+ and Na^+ occurred upon heat treatment at 400-500°C, which leads the loss of antibacterial property [39]. Furthermore, ion exchange process between Ag^+ and Na^+ results in formation of non-bridging oxygens in

the glass matrix and silver ions are bonded to these non-bridging oxygens, which helps stabilization of silver in ionic state and thus retards the reduction of silver ions to metallic ones [40].

Crystallization of silica matrix

Incorporation of silver in silica matrix affects the crystallization behavior of silica matrix. It has been proposed that ionic vibrations of silver colloids at metal- glass interface disrupt the amorphous network and initiates atomic arrangment for crystallization. It was also observed that the effect of silver on crystallization of silica matrix became more noticable with increasing silver concentration and heat treatment temperature [41].

1.3 Objective of the thesis

The aim of the current study is to address and solve some of the aforementioned problems in obtaining chemically durable sol-gel derived antibacterial powders and coatings. The specific objectives of this work can be outlined as follows:

- Synthesis of silver doped silica based materials for antibacterial use both in powder and coating form.
- Achieving chemical and structural changes on these functional surfaces and, determination of the effects of these alterations on antibacterial activity.
- Investigation of chemical durability of antibacterial materials under controlled and defined environmental mediums.

The effects of "performance-related material properties" on antibacterial activity, chemical durability and degradation of the coatings will be determined for the proposed system. After these observations and determinations, general process parameters will be defined for the development of antibacterial and highly durable materials. There are some critical material properties required for effective antibacterial use. These

properties may change the functional antibacterial activity (release of Ag^+ ion or physical contact mechanism between Ag^+ and bacteria) or may affect optical properties of coatings such as transparency under visible light.

1.4 References

[1] Pal S, Tak YK and Song JM,"Does the antibacterial activity of silver depend on the shape of nanoparticle? A study of the gram negative bacterium Escherichia coli", Appl. Environ. Microbiol 73(6), 1712-1720 (2007).

[2] Fayaz AM, Balaji K, Girilal M, Yadav R, Kalaichelvan PT and Venketesan R, "Biogenic synthesis of silver nanoparticles and their synergistic effect with antibiotics: a study against gram-positive and gram-negative bacteria", Nanomedicine 6(1), 103-109 (2010).

[3] Elechiguerra JL, Burt JL, Morones JR, Camacho-Bragado A, Gao X, Lara HH and Yacaman MJ, "Interaction of silver nanoparticles with HIV-1", J. Nanobiotechnol., 3, 6 (2005).

[4] Sang F, Kim W, Jung, JH, Lamsal K, Kim YS, Min JS and Le YS, "Antifungal effects of silver nanoparticles (AgNPs) against various plant pathogenic", Mycobiology, 40(1), 53–58 (2012).

[5] Chen J, Han CM, Lin XW, Tang ZJ and Su SJ, "Effect of silver nanoparticle dressing on second degree burn wound", 44(1), 50-52 (2006).

[6] Clement JL, Jarrett PS, "Antibacterial silver", Met.-based Drugs 1, 467–482 (1994).

[7] Feng QL, Wu J, Chen GQ, Cui FZ, Kim TN and Kim JO, "A mechanistic study of the antibacterial effect of silver ions on Escherichia coli and Staphylococcus aureus", J. Biomed. Mater. Res., 52, 662–668 (2000).

[8] Kell DB, Kaprelyants AS, Weichart DH, Harwood CR and Barer MR, "Viability and activity in readily culturable bacteria: a review and discussion of the practical issues", Antonie van Leeuwenhoek, 73,169-187 (1998).

[9] Morones JR, Elechiguerra JL, Camacho JB and Ramirez JT, " The bactericidal action of silver nanoparticles", Nanotechnol., 16, 2346-2353 (2005).

[10] Egger S, Lehmann RP, Height MJ, Loessner MJ and Schuppler M, "Antimicrrobial properties of a novel silver-silica nanocomposite material", Appl. Environ Microbiol., 75(9), 2973-2976 (2009).

[11] Bansal V, Li V, O'Mullane AP and Bhargava SK, "Shape dependent electrocatalytic behaviour of silver nanoparticles", Cryst. Eng. Comm.12(12), 4280–4286 (2010).

[12] Bae E, Park HJ, Lee J, Kim Y, Yoon J, Park K, Choi K and Yi J, "Bacterial cytotoxicity of the silver nanoparticle related to physicochemical metrics and agglomeration properties", Environ. Toxicol. Chem., 29, 2154–2160 (2010).

[13] Kawashita M, Tsuneyama S, Miyaji F, Kokubo T, Kozuka H and Yamamoto K, "Antibacterial silver-containing silica glass prepared by sol-gel method", Biomaterials, 21(4), 393-398 (2000).

[14] Tian XS, Lv CJ and Zhang GL, "Preparation and antibacterial activity of Al_2O_3-ZrO_2 Carrying Ag^+", Appl. Mech. Mater., 55-57, 1464-1467 (2011).

[15] Akhavan O, "Lasting antibacterial activities of Ag–TiO_2/Ag/a-TiO_2 nanocomposite thin film photocatalysts under solar light irradiation", J.Coll. Inter. Sci. 336 117-124 (2009).

[16] Shameli K, Ahmad MB, Zargar M, Yunus WM and Ibrahim NA, "Fabrication of

silver nanoparticles doped in the zeolite framework and antibacterial activity", Int J Nanomedicine 6, 331-341 (2011).

[17] Kobayashi Y, Katakami H, Mine E, Nagao D, Konno M and Liz-Marzán LM, "Silica coating of silver nanoparticles using a modified Stober method", J. Colloid. Interface Sci., 283(2), 392-396 (2005).

[18] Palomba M, Carotenuto G, Cristino L, Di Grazia MA, Nicolais F and Nicola SD, "Activity of Antimicrobial Silver Polystyrene Nanocomposites", J. Nanomat. Journal of Nanomaterials, 2012, 1-7 (2012).

[19] Durucan C, Akkopru B, "Effect of calcination on microstructure and antibacterial activity of silver-containing silica coatings", 93, 448-458 (2010).

[20] Ahmed AA and Allah EWA, "Origin of Absorption Bands Observed in the Spectra of Silver ion-exchanged soda–lime–silica glass", J. Am. Ceram. Soc., 78, 2777–2784 (1995).

[21] Tanahashi I, Manabe Y and Tohda T, Sasaki S, Nakamuro A, "Optical nonlinearities of Au/SiO_2 composite thin films prepared by a sputtering method", J. Appl. Phys., 79, 1244-1249 (1996).

[22] Matsunami N and Hosono H, "Colloid formation effects on depth profile of implanted Ag in SiO_2 glass", Appl. Phys. Lett. 63, 2050-2052 (1993).

[23] Desai NP, Hossainy SFA, Bubbell JA, "Surface-immobilized polyethylene oxide for bacterial repellence", Biomaterials, 13, 417-420 (1992).

[24] Kikuchi Y, Sunada K, Iyoda T, Hashimoto K, Fujishima A, "Photocatalytic bactericidal effect of TiO_2 thin films: dynamic view of the active oxygen species responsible for the effect", J. Photochem. Photobiol. A., 106, 51-56, (1997).

[25] Nablo BJ, Chen TY, Schoenfisch MH, "Sol-gel derived nitric oxide releasing materials that reduce bacterial adhesion", J. Am. Chem. Soc., 123, 9712-9713, (2001).

[26] Pai MP, Pendland SL, Danziger LH, "Antimicrobial-coated/bonded and impregnated intravascular catheters", Ann. Pharmother, 35, 1255-1263 (2001).

[27] Adams AP, Santschi EM, Mellencamp MA, "Antibacterial properties of a silver chloride-coated nylon wound dressing", Vet. Surg., 28, 219-225 (1999).

[28] Gottardi W, "Iodine and iodine compunds", In Block SS, editor, "Disinfection, Sterilization and Preservation", Philadelphia, USA: Lea Febiger, page 152-166 (1991).

[29] Prabhu S, Poulose EK, "Silver nanoparticles: mechanism of antimicrobial action, synthesis, medical applications, and toxicity effects", Inter. Nano Lett., 2:32, 1-10 (2012).

[30] Bruni S, Cariati F, Casu M, Lai A, Musinu A, Piccaluga G, Solinas S, "IR and NMR study of nanoparticle support interactions in Fe2 O3 –SiO2 nanocomposite prepared by a sol–gel method", Nanostruct. Mater., 11, 573-586 (1999).

[31] Jeon HJ, Yi SC, Oh SG, "Preparation and antibacterial effects of Ag–SiO2 thin films by sol–gel method", Biomaterials , 24, 4921-4928, (2003).

[32] Menning M, Schmidt M, Schmidt H, "Synthesis of Ag-colloids in sol-gel derived SiO_2 coatings on glass", J. Sol-gel Sci. Technol., 8, 1035-1042 (1997).

[33] Ritzer B, Villegas MA, Navarro F, "Influence of temperature and time on the stability of silver in silica sol-gel glasses", J. Sol-gel Sci. Technol., 8,917-921, (1997).

[34] Villegas MA, García MA, Paje SE, Lopis JL, "Parameters controlling silver nanoparticle growth in sol–gel silica coatings", Mater. Res. Bull., 40, 1210–1222 (2005).

[35] Suyal G, Menning M, Schmidt H, "Effect of Glass Substrates on the Formation of Gold-Silver Colloids in Nanocomposite Thin Films", J. Sol-gel Sci. Technol., 29, 11-18, (2004).

[36] Akhavan O, Moshfegh AZ, Hosseini AA, "Size variation and optical absorption of sol-gel Ag nanoparticles doped SiO_2 thin film", Thin Sol. Films, 515, 771 – 774 (2006).

[37] Li W, Seal S, Megan E, Ramsdell J, Scammon K, Lelong G, Lachal L, Richardson KA, "Physical and optical properties of sol-gel nano-silver doped silica film on glass substrate as a function of heat-treatment temperature", J. Appl. Phys., 93, 9553-9561 (2003).

[38] De G, Licciulli A, Massaro C, Tapfer L, Catalano M, Battaglin G, Meneghini C, Mazzoldi P, "Silver nanocrystals in silica by sol-gel processing", J. Non-Cryst. Sol., 194, 225-234 (1996).

[39] García MA, García-Heras M, Cano E, Bastidas JM, and Villegas MA, Sada C, De Marchi G, Battaglin G, and Mazzoldi P, "Photoluminescence of silver in glassy matrices", J. Appl. Phys., 96, 3737-3741 (2004).

[40] Wang J, Wu GM, Shen J, Yang TH, Zhang QY, Zhou B, Deng ZS, Fan B, Zhou DP, Zhang FS, "Scratch-resistant improvement of sol-gel derived nano-porous silica films", J. Sol-gel Sci. Technol, 18, 219-224 (2000).

[41] Ortega-Zarzosa G, Martínez JR, Robledo-Cabrera A, Martínez- Castañón GA, Sánchez-Loredo MG, Ruiz F, "Annealing behavior of silica gel powders modified

with silver crystalline aggregates", J. Sol-gel Sci. Technol., 27, 255-262 (2003).

CHAPTER 2

PREPARATION and MICROSTRUCTURE of SOL-GEL DERIVED SILVER-DOPED SILICA

2.1 Introduction

Preparation of nanosized metal-doped silica and glasses has attracted great attention in the past few years. Besides their high surface area serving for high functional properties, these metal-silica hybrids have chemical and physical properties differing from those of the bulk form. They have potential for applications in optics, optoelectronics, and catalysis and as antibacterial materials. Variety of different techniques has been used to introduce silver or other noble metals into silicate glasses such as sputtering [1], ion implantation [2, 3], and ion exchange [4, 5]. The sol-gel method is also used for preparing silver-doped silica, where silver particles are incorporated into the matrix by dissolving silver salts in one of the aqueous sol-gel precursors [6–11]. Compared to other methods, the sol-gel method provides a practical way of achieving uniform distribution of silver particles in both pure and organically modified silica matrices. Sol-gel also enables control of the size, the distribution, and the chemical state of silver; all of which are critical for technical applications. Sol-gel, a low temperature process, also provides easy control of silver concentration and the possibility to add reducing and oxidizing agents in small concentrations to modify the chemical state of silver.

Some recent works report preparation and physical properties of silica containing different amounts of silver in various chemical states by sol-gel method, both in powder [12–18] and coating form [19–26]. However, little attention has been paid to understand

the effects of microstructural properties of the silica matrix and its effect on the formation of silver particles. Given the relative important optical and biotechnological applications of silver- doped glassy silica further understanding of the physical properties/characteristics controlling the performance is essential. Optical and antibacterial properties as well as long-term chemical durability are directly related to the silver size and its distribution along with the porosity and chemical state of the silica matrix.

In the present study, preparation of silver-doped silica powders by the sol-gel technique has been reported. We attempted to control the particle size of silver nanoparticles, chemical state, and microstructural properties of silica matrix by changing the catalysis mechanism in the sol-gel reactions and by employing different calcination temperatures. The formation silver-doped silica powders at various calcination temperatures and changes in the chemical nature of the silica matrix by thermal treatments for these two specific preparation conditions were examined using a XRD, BET and UV–Vis. Silver particle formation mechanism in microstructurally different silica matrices and changes in the silica matrix upon heat treatments are discussed.

2.2 Experimental procedure

2.2.1 Preparation of silver-doped sol-gels

Powder samples with different silver concentrations were prepared. The starting solution used to prepare the samples consisted of mixtures of tetraethyl orthosilicate (TEOS, $Si(OC_2H_5)_4$, Aldrich), silver nitrate ($AgNO_3$, Aldrich), ethanol (C_2H_5OH, Merck) and distilled water. Two different routes were used. In first route called ‘‘acid-catalysis’’, only HNO_3 catalyst was used. In the second route hereafter named as ‘‘acid/base catalysis’’ a two-step acid/base (HNO_3 and NH_4OH) catalysis was performed. All concentrations are presented in molar ratio.

Acid-catalyzed sol-gels: In this route, a set of sol-gel mixtures with two different silver concentrations; a moderate concentration, $[AgNO_3]/[TEOS] = 0.015$ and higher concentration $[AgNO_3]/[TEOS] = 0.060$ were prepared. The molar ratio of the solgel mixtures and other processing details for this set are shown in Table 1. In the first step starting solutions were obtained by mixing the required amount of $AgNO_3$ and distilled water. Then 0.1 M HNO_3 solution and half of the ethanol were added to the starting solution. This mixture was stirred for 20 min at room temperature to form solution-A. In another beaker, TEOS and the remaining portion of ethanol were mixed for 20 min to obtain solution-B then solution-A was slowly added into solution B under stirring. After complete addition, the mixture was stirred for 100 min at room temperature and poured into polystyrene test tubes and sealed with Parafilm for gelation. Gelation occurred in air after 4–5 days.

Acid/base catalyzed sol-gels: Sol-gel mixtures as listed in Table 2.1 with low concentration, i.e., $[AgNO_3]/[TEOS] = 0.0037$ and moderate concentration, $[AgNO_3]/[TEOS] = 0.015$ were prepared. The higher silver concentrations were not prepared because these higher silver concentrations resulted in inhomogeneous mixing and phase separation of silver precipitates. In the first step, the required amount of $AgNO_3$ and H_2O is stirred at room temperature for 20 min to form solution-C. In another beaker, TEOS–ethanol solution, solution-D, was mixed. Then 0.1 M HNO_3 solution was added drop-wise into TEOS containing solution (solution-D) to adjust the pH to a value of pH = 1. The pH adjusted solution-D was stirred for 10 min followed by dropwise addition of 0.75 M NH_4OH solution to increase the pH to a value of pH = 2.0. At this time solution-C is then poured into solution-D. After mixing for 10 min, the pH of the mixture is adjusted to 5.0–5.5 by NH_4OH addition. The pH value of the solution-D at the time of the addition of solution-C was found to be critical factor during preparation.

When the $AgNO_3$–H_2O solution (solution C) was poured into TEOS–EtOH solution at pH lower than two or higher than four, small black precipitates were formed, leading to an inhomogeneous mixture. The optimum pH value of solution-D, which gives a homogenous solution upon mixing, was found as pH 2.7–2.8. Under these conditions,

Table 2.1 Formulations and approximated gelation times for silver-doped silica gels obtained (a) by acid-catalysis and (b) by acid/base-catalysis route. All concentrations shown are in molar ratio.

(a)

Acid Catalysis	**[$AgNO_3$]/[TEOS]=0.015**	**[$AgNO_3$]/[TEOS]=0.060**
Formulation	TEOS:$AgNO_3$:C_2H_5OH:H_2O : HNO_3	TEOS:$AgNO_3$:C_2H_5OH:H_2O: HNO_3
(Molar ratio)	1 : 0.015 : 2 : 8 : 0.015	1: 0.060 : 2 : 8: 0.015
Gelation time	4-5 days	4-5 days

(b)

Acid/base Catalysis	[$AgNO_3$]/[TEOS]=0.0037	[$AgNO_3$]/[TEOS]=0.015
Formulation	TEOS:$AgNO_3$:C_2H_5OH:H_2O: HNO_3 : NH_4OH	TEOS:$AgNO_3$:C_2H_5OH:H_2O:HNO_3: H_4OH
(Molar ratio)	1:0.0037:3.8:2:0.03:0.02	1:0.015:3.8:2:0.03:0.02
Gelation time	40 min.	40 min.

the final solution was free of any small dark precipitates and did not show a color change. Final sol-gel mixtures were poured into polystyrene test tubes and sealed with Parafilm. The complete gelation in air and syneresis were observed in 1 h and 3–4 h, respectively.

2.2.2 Chemical durability test of the silver-doped silica powders

Acid/base catalyzed gels were used during chemical durability test. Acid/base catalyzed gels with [AgNO3/TEOS=0.015] molar ratio were exposed to different aggressive mediums (pH=3, pH=5.5, pH=10). Erosion of silver from silica matrix into solution were determined by ICP-MS techniques. For the preperation of acidic solution, HCl (37%, Merck) and for basic solution, NH_4OH (15 M, Sigma-Aldrich) were used.

2.2.3 Antibacterial activity test of the silver-doped silica powders

Acid and Acid/base catalyzed gels with [$AgNO_3$]/[TEOS]=0.015 molar ratio were exposed to antibacterial performance test against *Escheria Coli*. Samples calcined at 200 ºC nad 800 ºC for two hours were used. Powders were presse at 5 kpa for 20 sec to form pellets. Final dimension of pellet was 3 and 8 mm in thickness and Radius, respectively. Then these pellets were placed in agar plates containing bacteria colonies and incubated for 24 hours. The reduction in the bacteria colony number was determined. Silica powders in the pellet form were also used as control sample during antibacterial performance test.

2.3 Characterization

2.3.1 XRD

X-ray diffraction analysis of the powder samples was performed using a Rigaku X-ray diffractometer D/Max-2000 PC. X-ray source was Ni-filtered CuKα radiation. The X-ray source operating voltage was 40 kV and the scan rate was 2º/min. The silver particle size was estimated by the Scherrer equation by analyzing the half-width broadening of the (111) diffraction peak [27].

2.3.2 Optical absorption

The optical absorbance of the powder gel products was measured using an ultraviolet visible diffusive reflection spectrometer (Varian Bio 100 UV–Vis Spectrophotometer) in the wavelength range of 200–800 nm. In a typical experiment transmission measurements were performed using constant amount of powder sample suspended in millipore water in a standard quartz cuvette. A sol-gel derived pure silica glass powder was used as a reference sample, to evaluate the background contribution.

2.3.3 Microstructural analysis

The pore sizes and distributions were determined using Quantachrome Autosorb-1-C/MS Model BET system according to BJH model. The analysis was carried out with approximately 0.3 g of sample using nitrogen as the absorbing gas and with helium flow as the evacuating gas.

2.4 Results

2.4.1 XRD analyses

Acid-catalyzed sol-gels: Figure 2.1 shows the XRD patterns of the acid-catalyzed samples of two different concentrations after heat treatment at 200 ºC, 400 ºC, 600 ºC and 800 ºC. The insets show the XRD pattern of sol-gel derived pure silica powder calcined for 2 h at 600ºC for comparison. Figure 2.1a presents the XRD patterns of samples containing moderate silver dopant concentration of $[AgNO_3]/[TEOS] = 0.015$ and Figure 2.1b shows the XRD patterns of samples containing higher silver $[AgNO_3]/[TEOS] = 0.060$. As shown in Figure 2.1a for moderate silver containing samples after heat treatment at 200 ºC, 400 ºC and 600 ºC only a broad peak representing the amorphous silica network is present. No other peaks including any peak for a silver phase are present. Heat treatment at 800 ºC leads to crystallization of the amorphous silica to cristobalite. In addition to the cristoballite peak, four peaks assigned to metallic silver at around 38º, 45º, 64º and 77º are present. XRD patterns for high silver containing samples as shown in Figure 2.1b indicate the presence of silver after a heat treatment at 600 ºC as well as at 800 ºC. Diffraction patterns of samples with $[AgNO_3]/[TEOS] = 0.060$ silver content heat treated at 800 ºC show an increase in theintensity of diffraction lines of silver compared to those of the same composition calcined at 600 ºC. Another distinction between these sets with varying silver concentration is the difference in crystallization trend of the silica matrices, which is promoted by an increase in silver amount. For acid-catalyzed silica with

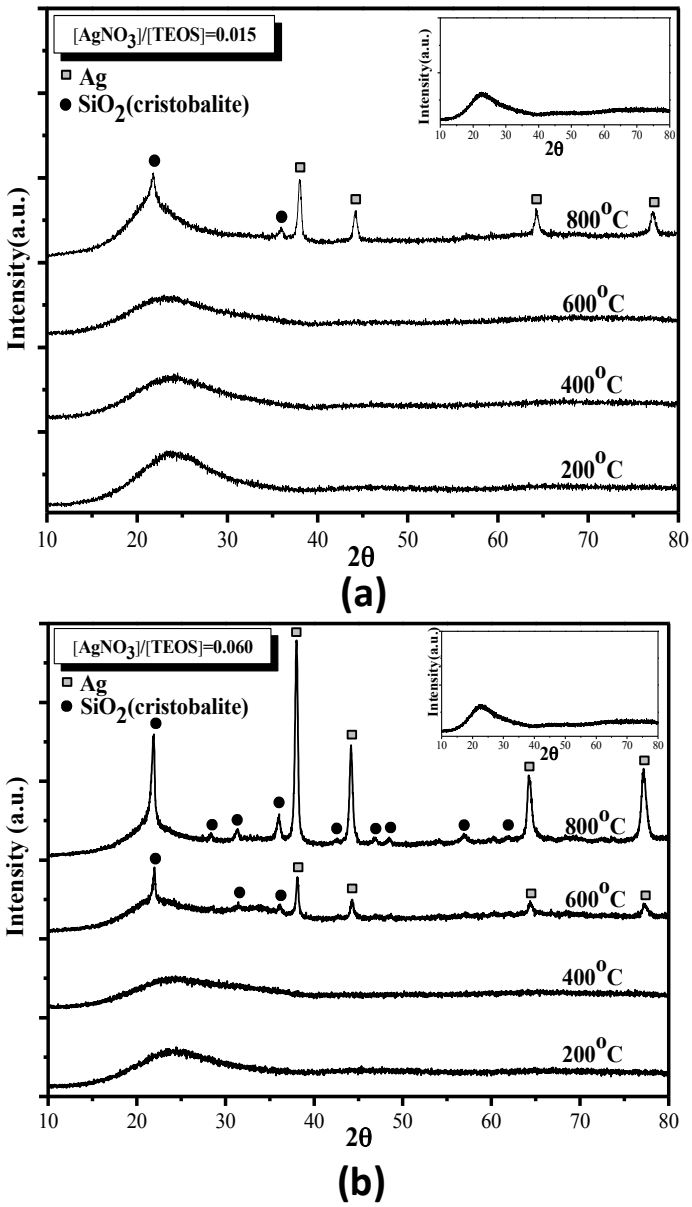

Figure 2. 1 X-ray diffraction patterns of silver containing silica gels prepared by acid-catalysis process with two different concentration (a) $[AgNO_3]/[TEOS]=0.015$,(b) $[AgNO_3]/[TEOS]=0.060$ heat treated for 2 h at different temperatures. The insets show the XRD pattern of undoped sol-gel derived silica calcined for 2h at 600°C.

$[AgNO_3]/[TEOS]$ = 0.060 crystallization to, cristoballite is observed at 600 ºC, whereas for less silver containing gels with $[AgNO_3]/[TEOS]$ = 0.015 crystallization is not observed until 800 ºC.

The average particle size of the silver particles formed after different heat treatments is shown in Table 2.2. For moderate of silver containing gels ([$AgNO_3$]/[TEOS] = 0.015), the average size of the silver particles was 24 ± 2 nm after heat treatment at 800 ºC. In high silver containing gels ([$AgNO_3$]/[TEOS] = 0.060) samples, the average particle sizes were 28 ± 2 nm and 30 ± 2 nm, after heat treatments at 600 ºC and 800 ºC, respectively.

Acid/base catalyzed sol-gels: Figure 2.2 shows the XRD patterns of two-step acid/base catalyzed gels with two different silver concentrations after heat treatment at 200 ºC, 400 ºC, 600 ºC and 800 ºC. Again the insets show the XRD pattern of sol-gel derived undoped silica after 2 h of calcination at 600 ºC. Figure 2.2a shows the XRD patterns for gels with a concentration of [$AgNO_3$]/[TEOS] = 0.0037 and Figure 2.2b shows the XRD patterns for gels with [$AgNO_3$]/[TEOS] = 0.015. For acid/base catalyzed gels with [$AgNO_3$]/[TEOS] = 0.0037 only an amorphous phase is observable up to 600 ºC. Crystallization of silica starts at around this temperature as revealed by a very weak intense peak distinguishable at 22º overlapping with the broad amorphous silica peak. After calcination at 800ºC, the XRD pattern shows only one small silver peak at around 38ºcorresponding to (111) diffraction of silver, as well as intense diffraction lines of cristobalite. For the acid/base catalyzed gel with [$AgNO_3$]/[TEOS] = 0.015 only a broad amorphous peak up to 200 ºC is visible. After firing at 400 ºC, in contrast to the acid-catalyzed gels with the same silver concentration acid/base catalyzed gels show a diffraction peak of silver metal. At 400 ºC, only one weak silver metal peak at around 38º, corresponding to the most intense (111) diffraction plane of silver, is observable. Calcination temperatures of 600 ºC and 800 ºC resulted in a gradual increase in the intensity of silver peaks and additional silver peaks are observed. Transformation of amorphous silicato cristobalite occurs after a heat treatment at 600 ºC. The average silver particle sizes for this set are listed in Table 2.2.

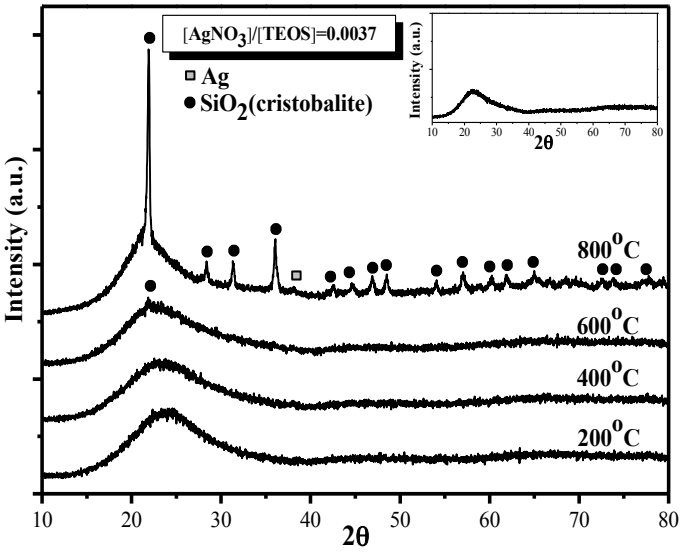

(a)

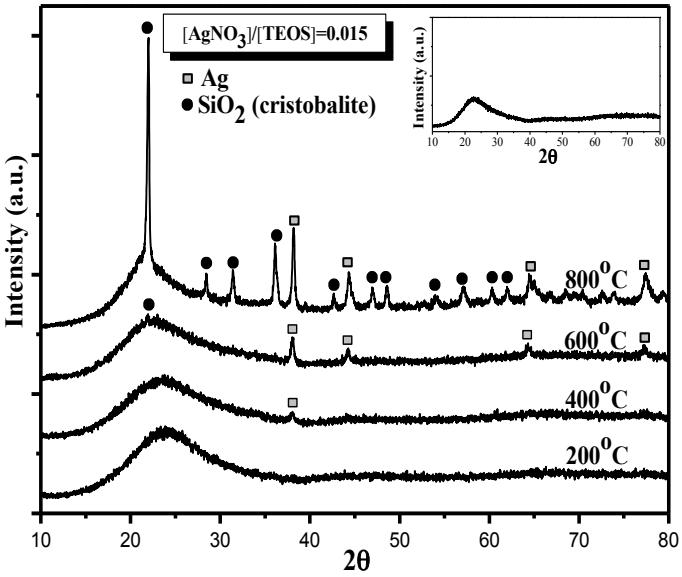

(b)

Figure 2. 2 X-ray diffraction patterns of silver containing silica gels prepared by acid/base catalysis process with two different concentration (a) $[AgNO_3]/[TEOS]= 0.0037$, (b) $[AgNO_3]/[TEOS]=0.015$ heat treated for 2 hours at different temperatures. The insets show the XRD pattern of undoped sol-gel derived silica calcined for 2h at 600° C.

Table 2.2 Average diameters of silver particles in silica gels after calcination for 2 hours at different temperatures.

Sol-gel Formulation (Calcination Temperature)	**Particle size (nm)**
Acid-catalyzed gels	
$AgNO_3$/TEOS=0.015 (800ºC)	**24± 2**
$AgNO_3$/TEOS=0.060 (600ºC)	**28± 2**
$AgNO_3$/TEOS=0.060 (800ºC)	**30± 2**
Acid/base-catalyzed gels	
$AgNO_3$/TEOS=0.0037 (800ºC)	**n.a.**
$AgNO_3$/TEOS=0.015 (400ºC)	**19± 2**
$AgNO_3$/TEOS=0.015 (600ºC)	**30± 2**
$AgNO_3$/TEOS=0.015 (800ºC)	**32± 2**

n.a. : not available

In the low-silver containing sample ([$AgNO_3$]/ [TEOS] = 0.0037), the average size of silver colloids could not be determined because of very small peak resolution. For moderate amount silver containing gels ([$AgNO_3$]/ [TEOS] = 0.015) the average particle size are 19 ± 2 nm, 30 ± 2 nm and 32 ± 2 nm, after heat treatments at 400 ºC, 600 ºC and 800 ºC, respectively. Higher calcination temperature resulted in slightly larger silver particle size.

2.4.2 BET analysis

Figure 2.3 shows the nitrogen gas adsorption isotherms for silver-doped silica gels after calcination at different temperatures. Average pore size and distribution are both presented. The silver concentration was [$AgNO_3$]/ [TEOS] = 0.015 in all cases and all samples were calcined for 2 h. For the acid-catalyzed gels, after calcination at 200 ºC, the average pore size and surface area were <25 Å and 325 m^2/g, respectively. The average pore size and surface area do not change remarkably with increasing calcination temperature; for both calcination treatments at 400 ºC and 600 ºC, surface area and

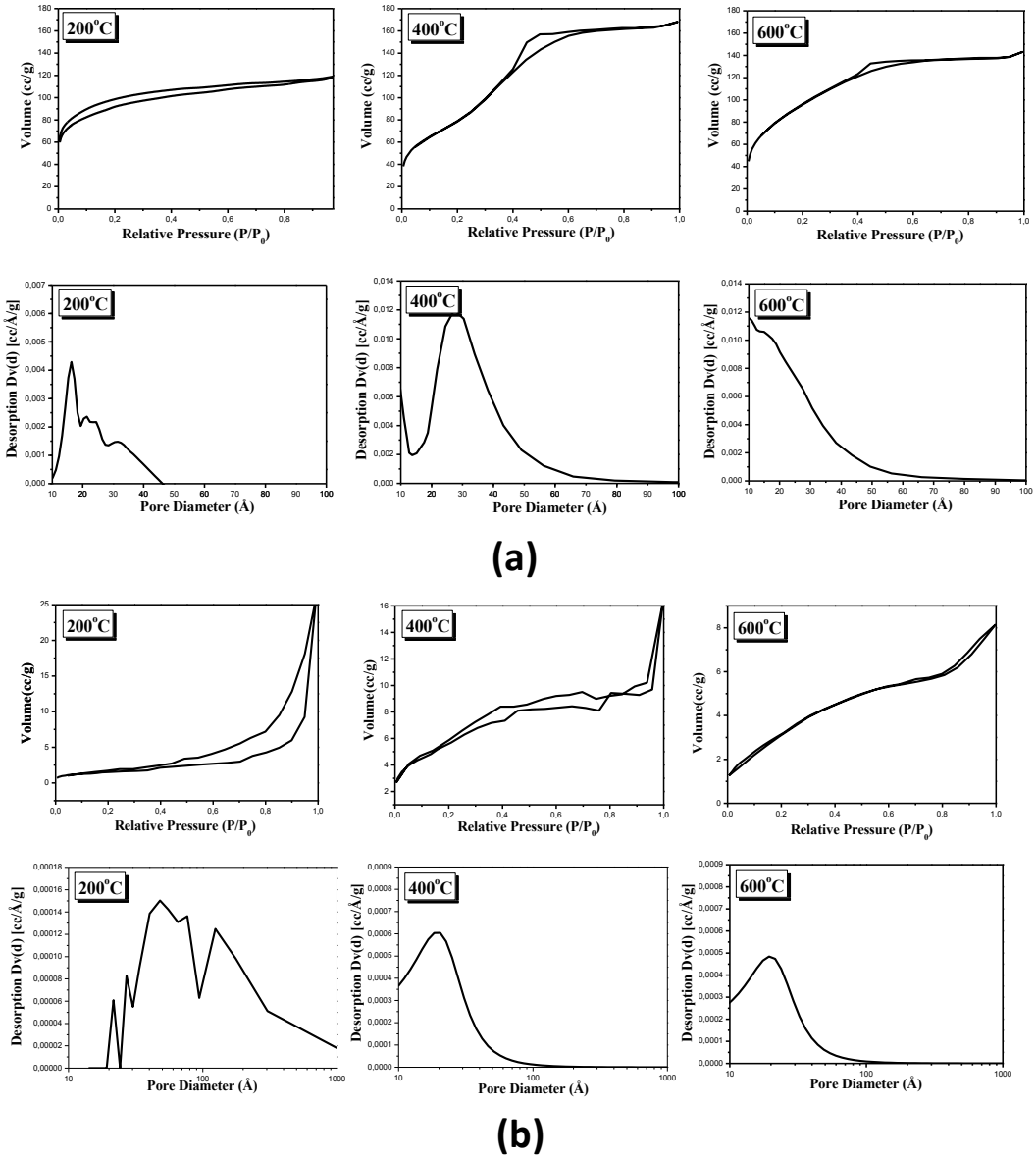

Figure 2. 3 Nitrogen adsorption/desorption isotherms and pore size distribution for silver doped silica prepared, (a) by acid catalysis route with [AgNO3]/[TEOS] = 0.015 calcined for 2 h at 200 ºC, 400 ºC and 600 ºC; (b) by acid/base catalysis route with [AgNO3]/[TEOS] = 0.015 calcined for 2 h at 200 ºC, 400 ºC and 600 ºC. The BJH average pore diameters are shown on pore size distribution graphs.

average pore size were found at around 310–345 m^2/g and <25 Å . For acid/base catalyzed gels on the other hand porosity and surface area both change with calcination temperature; the average pore size and surface area after calcination at 200 ºC were

determined as 250 Å and 5.2 m^2/g. The average pore size was found as 75 Å and 55 Å after calcination at 400 ºC and 600 ºC, respectively. The surface area for the samples calcined at 400 ºC and 600 ºC were higher than that for 200 ºC reaching to a value in the range of 15–20 m^2/g. For both synthesis routes, samples calcined at 800 ºC did not exhibit micro- or meso-porosity measurable with nitrogen gas.

2.4.3 UV–Vis analysis

Figure 4 shows the absorption spectra for the acid and acid/base catalyzed gels with two different silver concentrations, after heat treatment at 200 ºC, 400 ºC, 600 ºC and 800 ºC. Figure 4a presents the spectra for acid catalyzed gel with a silver concentration of $[AgNO_3]/[TEOS]$ =0.015. Heating at about 800 ºC induced the evolution of a peak at around 412 nm due to the surface plasmon resonance of the silver particles. Figure 4b shows the optical absorption spectra for acid-catalyzed gel with an initial concentration of $[AgNO_3]/[TEOS]$ = 0.060. Heating at about 600 ºC induced the evolution of a small peak at around 412 nm. Further increase in the annealing temperature to 800 ºC drastically increased the intensity of the surface plasmon resonance peak. Figure 4c shows the optical absorption spectra of the acid/base catalyzed gel with a silver concentration of $[AgNO_3]/[TEOS]$ = 0.0037. The surface plasmon resonance of silver is hardly observable even after heating to 800 ºC. Figure 4d shows the optical absorption spectra for the acid/base catalyzed gel with $[AgNO_3]/[TEOS]$ = 0.015. Heating to 200 ºC induced the evolution of the surface plasmon peak of silver at 412 nm, which appears as a wide shoulder for samples calcined at 200 ºC and 400 ºC. It took a well-defined peak shape when the calcination temperature was raised to 600 ºC. After heat treatment at 800 ºC, the surface plasmon resonance peak for silver was still present.

2.4.4 Chemical durability test results of silver-doped silica powders

Figure 2.5 shows the ICP-MS results indicating the effect of pH medium on erosion of silver. ICP-MS analysis were performed after exposing gels to aggressive acidic or basic medium for 2 months. As shown in Figure 2.5, the amount of Ag^+ corroded from silica

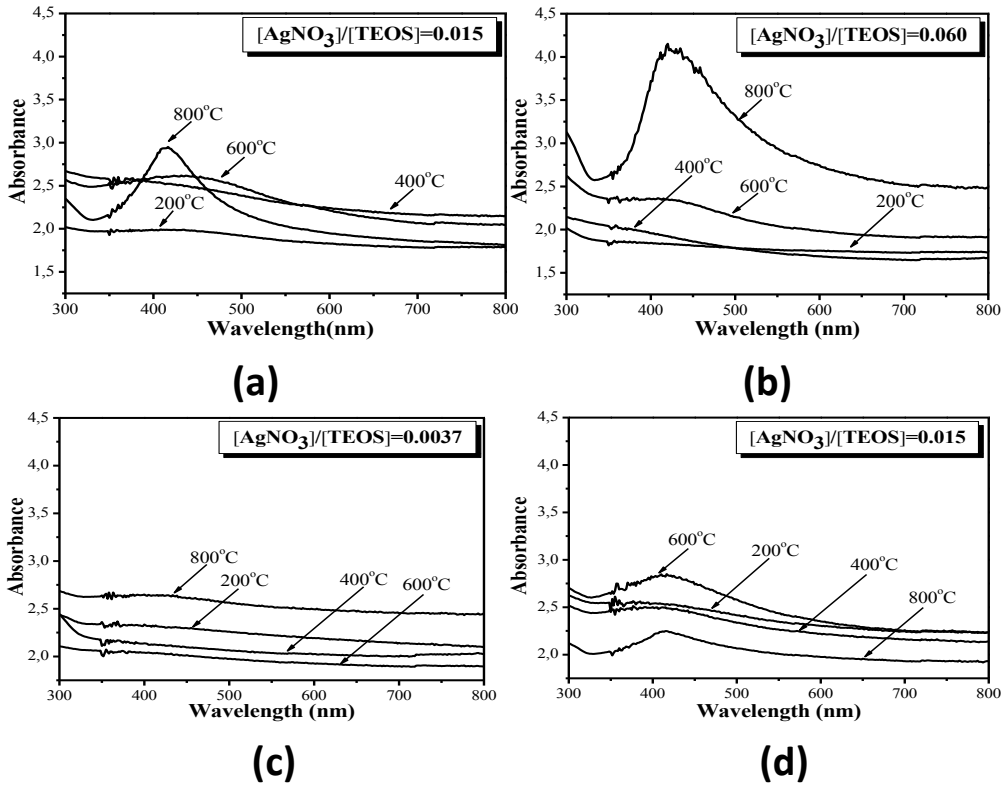

Figure 2. 4 UV-Vis absorption spectra of silver doped silica prepared by acid catalysis route with (a) $[AgNO_3]/[TEOS]=0.015$ (b) $[AgNO_3]/[TEOS]=0.060$, and by acid/base-catalysis route (c) $[AgNO_3]/[TEOS]=0.0037$, (d) $[AgNO_3]/[TEOS]=0.015$ after calcination for 2 hours at 200°, 400°, 600° and 800°C.

matrix during acidic treatment, is 1.97 mg/lt, whereas, eroded Ag^+ amount under basic treatment is 0.894 mg/lt. Thus, acid/base catalyzed gels has higher durability at higher pH values. Silver present in silica matrix can be corroded in two ways. First, erosion of silver occurs by decomposition of silica matrix in which Si-O bonds are hydrolyzed. This type of corrosion occurs when the OH^- ions in the medium is very high. In the second way, erosion of silver occurs by exchange mechanism between Ag^+ and H_3O^{+-} ions. It s widely accepted that the erosion of silver most likely occurs due to the decomposition of silica matrix. Since acid/base catalyzed gels have more open microstructure, the rate of exchange mechanism between Ag^+ and H_3O^- increases and thus enhancing corrosion of silver.

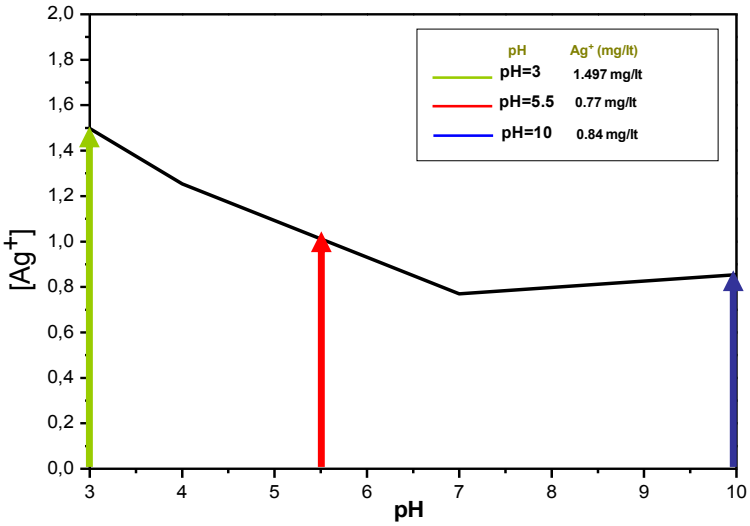

Figure 2. 5 Chemical durability test results of silver-doped silica powders produced by acid-base catalyzed method and calcined at 800 ºC for 2 hours after exposing to aggressive mediums (pH=3, 5.5, 10).

2.4.5 Antibacterial activity test results of silver-doped silica powders

Acid and Acid/base catalyzed gels with [AgNO3]/[TEOS]=0.015 calcined at 80 ºC and 800 ºC molar ratio were exposed to antibacterial test. Antibacterial test results of acid and acid/base catalyzed gels calcined at 80 ºC and 800 ºC are given in Figure 2.6. As shown in Figure 2.6, antibacterial activity is significantly affected by heat treatment temperature and production method. In these figures, white points represents the bacteria colonies. For both acid and acid/base catalyzed powders, antibacterial activity weakened with increasing cacination temperature.

2.5 Discussion

The most notable difference between the two processing routes is the total gelation time. The gelled state was achieved in 4–5 days for the acid-catalyzed process, whereas the

acid/base catalyzed system gelled in 40 min. This difference is due to achieving the optimum hydrolysis and condensation pH conditions in the case of two-step catalysis [28]. Another processing related distinction is the total silver amount that can be

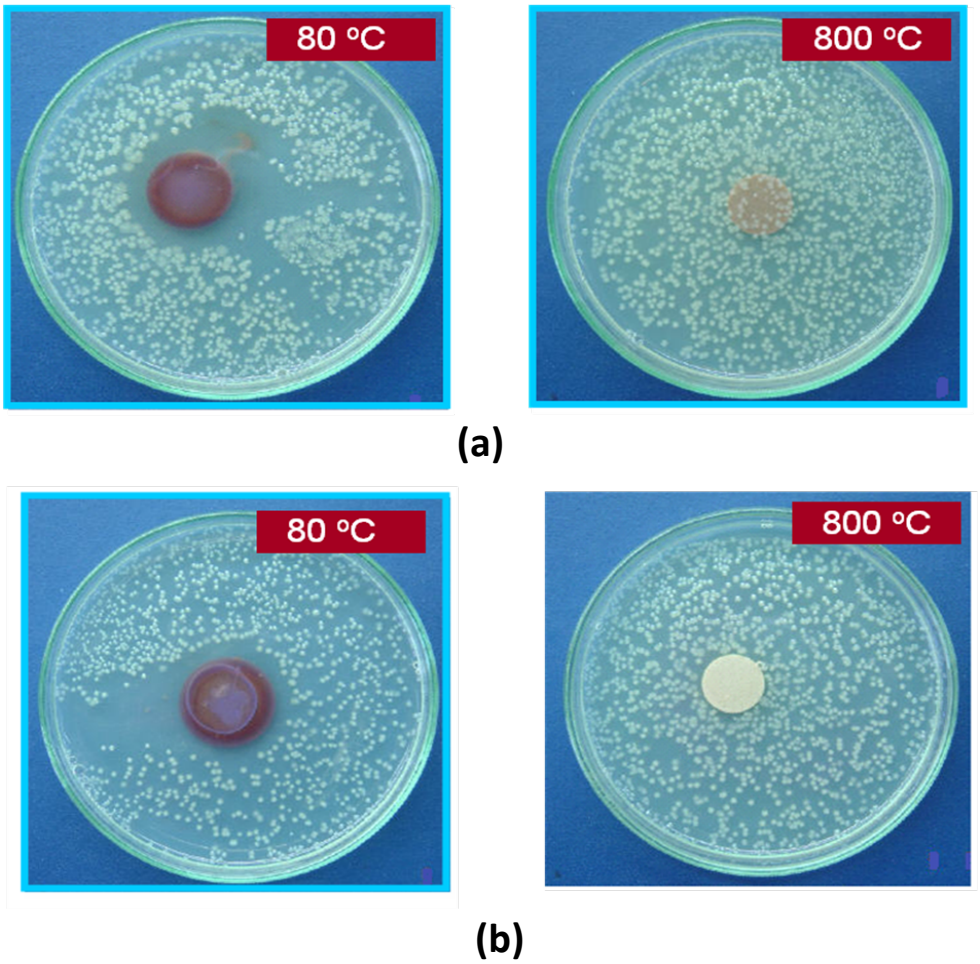

Figure 2. 6 Optical pictures showing antibacterial test results of silver doped silica powders produced by a) acid catalyzed, b) acid-base catalyzed methods, (white points represent the escheria-coli bacteria colonies).

incorporated into silica. For the two-step acid/base catalyzed route the maximum amount of silver that can be incorporated is at around a concentration corresponding $[AgNO_3]/[TEOS] = 0.015$. In the two-step acid/base catalyzed route; higher silver doping; i.e., $[AgNO_3]/[TEOS] > 0.015$ resulted in structurally inhomogeneous gels where phase separation of silver precipitates occurs. This essentially limited the

production of gels with higher amount of silver via two-step catalysis route.

For both synthesis routes acid and acid/base catalyzed gels, after a heat treatment in the range of 200 ºC–800 ºC silver nitrate ($AgNO_3$) in the gel should decompose at around 350 ºC expelling nitrate in the form of nitrogen gas and generating metallic silver particles in the silica matrix by spontaneous reduction of the silver ions. However XRD results revealed differences in the temperature required to form metallic silver particles due to differences in the processing route.

For the gels produced by acid-catalysis route, the silver is only observable after calcination at 800 ºC for moderate silver containing silica ([$AgNO_3$]/[TEOS] = 0.015). In the case of higher silver containing samples ([$AgNO_3$]/[TEOS]) = 0.060) of the same processing route, silver particles were formed at a lower calcination temperature of 600 ºC. But for both concentrations, no silver peak was observed for calcination temperatures of 400 ºC and lower. For acid/base catalyzed gels with low silver concentration ([$AgNO_3$]/[TEOS] = 0.0037) produced by the two-step catalyst method a silver peak in the XRD pattern is only present for samples calcined at 800 ºC. No silver peak is present for the samples calcined at 400 ºC or 600 ºC.

Absence of silver XRD peak for gels heat treated at lower temperatures may be due the amorphous silica matrix with a very broad peak overlapping to some extent with the silver peak which is in trace amount for detection by XRD. Therefore, missing silver peaks may be due to the intrinsic limitation of XRD itself as there is only limited amount of silver with an average size of 20–30 nm is available for detection. This is also supported by the optical absorption measurements. For instance, the XRD analysis of the acid-catalyzed gel with [$AgNO_3$]/[TEOS] = 0.015 heat-treated at 400 ºC and 600 ºC do not exhibit any silver peak. On the other hand, UV–Vis spectra of the silica gels ,which had been heat-treated at 400 ºC and 600 ºC show a shoulder centering around surface plasmon resonance peak position (Fig. 2.4 a). This suggests presence of metallic silver particles in the silicate gels after heat treatments even though they are absent in the XRD patterns. Same is valid for the acid/base catalyzed gel of the concentration

[$AgNO_3$]/[TEOS] = 0.0037, where no XRD peak is observable for samples calcined at 400 ºC and 600 ºC. But UV–Vis in Fig. 2.4 c shows the features resembling a wide and weak intensity peak for colloidal silver centered at 412 nm. The conflict between XRD and UV–Vis results for higher silver nitrate [$AgNO_3$]/[TEOS] = 0.015 containing set of acid/base-catalyzed gel is valid only for the sample calcined at 200 ºC. This gel calcined at 200 ºC does not exhibit any silver XRD peak but a silver surface plasmon resonance peak as shown in Figure 2.4 d. The XRD and UV–Vis for the samples calcined at higher temperatures (T > 400 ºC) indicate parallel results. This particular composition in fact leads to best efficiency in terms of metallic silver formation extent, i.e., with moderate silver loading and relatively low calcination temperature at around 400 ºC. This point will be clarified further in our discussion.

Differences in the processing route also lead to a different crystallizations trend for the glassy silica matrices. Based on the XRD results, for both processing routes, higher silver dopant leads to a promotion in the crystallization of the silica matrix into cristobalite. This effect is more evident for acid-catalyzed gel, in which crystallization of silica starts somewhere between 600 ºC and 800 ºC at a moderate silver concentration ([$AgNO_3$]/[TEOS] = 0.015). In contrast, for the silica with higher silver loading ([$AgNO_3$]/[TEOS] = 0.060) again formed by the acidcatalysis route, crystallization starts at a much lower temperature; somewhere between 400 ºC and 600 ºC. These acid-catalyzed gels differ in terms of total degree of crystallization achieved at maximum calcination temperature of 800 ºC. The cristobalite diffraction peak for the samples calcined at 800 ºC for the higher silver containing sample ([$AgNO_3$]/[TEOS] = 0.060) is much more intense compared to those of the lower silver containing gel ($AgNO_3$ /TEOS = 0.015). On the other hand crystallization of the acid/base catalyzed silica gel does not start until reaching to 600 ºC for both low ([$AgNO_3$]/[TEOS] = 0.0037) and moderate ([$AgNO_3$]/[TEOS] = 0.015) silver containing gels. At calcination temperature of 800 ºC higher silver containing gel has more intense cristobalite peak. Almost for every silver containing gel formulation the crystallization trend to cristobalite at 600 ºC is relatively higher than that in phase pure silica, as depicted by the insets in XRD figures. According to previously suggested model, improved crystallization of amorphous sol-

gel derived silica occurs due to presence of metallic silver particles. It is believed that metallic colloids disrupt the amorphous network and lead to ionic vibrations at the glass–metal interface, which initiate the atomic arrangement for crystallization [29]. The improved crystallization of silverdoped silica has been also related to heat localization effect, where each metallic particle acts as a local heating center in close approximation in the glassy matrix [30]. This type of arrangement reduces the kinetic barrier for crystallization of glassy silica matrix.

But in our case, in addition to silver concentration some other factors are also critical for the difference in silica crystallization degree. This is based on the fact that at the same silver concentration of $[AgNO_3]/[TEOS] = 0.015$ only acid/base catalyzed gel shows signs of limited crystallization. In addition, when 800 ºC XRD patterns are compared, acid/base catalyzed gel exhibits a much more intense cristobalite peak compared to that of acid-catalyzed gel. This observation suggests that another microstructural property controlling the crystallization behavior of the silica matrix (in addition to silver amount) is the porosity and its effect on the development of silver particles in silica during gel formation and subsequent thermal treatments. The BET isotherm for the acid-catalyzed gel in the fully dried state is indicative of a type-I microporous absorbent with an average pore size of <25 Å determined according to the BJH model. A type-IV isotherm typical of a mesoporous solid is observed for the two-step acid/based catalyzed gel with an average pore size of 250 Å exhibiting a more open microstructure. This effect is analogous to the pH effect on microstructure, well known for silica gels synthesized from silicon alkoxides [31]. Sol-gels formed under acid-catalyzed conditions are in the form of highly overlapping linear or randomly branched chain networks. During densification, this network further cross-links into a compact structure with limited free volume. For the acid/base catalyzed synthesis, as followed in rapid gelling silica the microstructure is more particulate, and the free volume is quite large. As revealed by the XRD data even the lowest silver doped acid/base catalyzed gel with bigger pores reaches a higher degree of crystallization at the highest calcination temperature (800 ºC) compared to the more dense acid-catalyzed gels with higher silver concentration. The crystallization of silica matrix is not only affected by silver concentration, but also by

silver size and porosity and its distribution in silica matrix which both strongly depend on the processing route.

It is clear, within the systems studied here, the porosity affects the silver particle size attained in silica in the asgelled state as well as during following thermal treatments. The average silver particle sizes shown in Table 2.2 imply that after heat treatment at 800 ºC for the gels with the same silver concentration of $[AgNO_3]/[TEOS] = 0.015$ are 24 ± 2 nm and 32 ± 2 nm, for acid and acid/base catalyzed gels, respectively. Even though the same amount of $AgNO_3$ is present in the starting sol-gel mixture, the acid/base catalyzed gel contains bigger silver particles or agglomerates of the colloidal metallic silver. As the structure becomes more open, there is a higher chance for precipitation of bigger silver colloids in the pores of silica or in the silicate network during hydrolysis and condensation. In this case, precipitation of silver occurs within silica the network and simultaneously and more probably on the pore surfaces as these sites are energetically more favorable due to higher free energy. During the heat treatments silver diffusion occurs faster due to more open space and the possibility of formation of silver aggregates increases as also suggested by other investigators [30, 32].

The improved crystallization trend of silica gels with big pores obtained by two-step acid/base catalysis can be explained with the help of the schematics shown in Fig. 2.7. This figure represents the microstructure of the selected silver-doped silica gels for the two gel processing routes employed in this study. The silver concentration was $[AgNO_3]/[TEOS] = 0.015$ for both gels. This figure also describes and summarizes the microstructural changes and suggests a mechanism for evolution of the final microstructure and chemical identity of the gels as a result of heat treatment from 200 ºC to 800 ºC. Figure 2.7 a and b represents the microstructure at 200 ºC for acid and acid/ base catalyzed gels, respectively. Figure 2.7 c and d represents the microstructure of the same gels after heat treatment at 800 ºC. The gels of different processing routes show two major differences at both conditions: (i) porosity—acid/base catalyzed gels typically have more pore space (mesoporous) and (ii) the silver particle size—acid/base

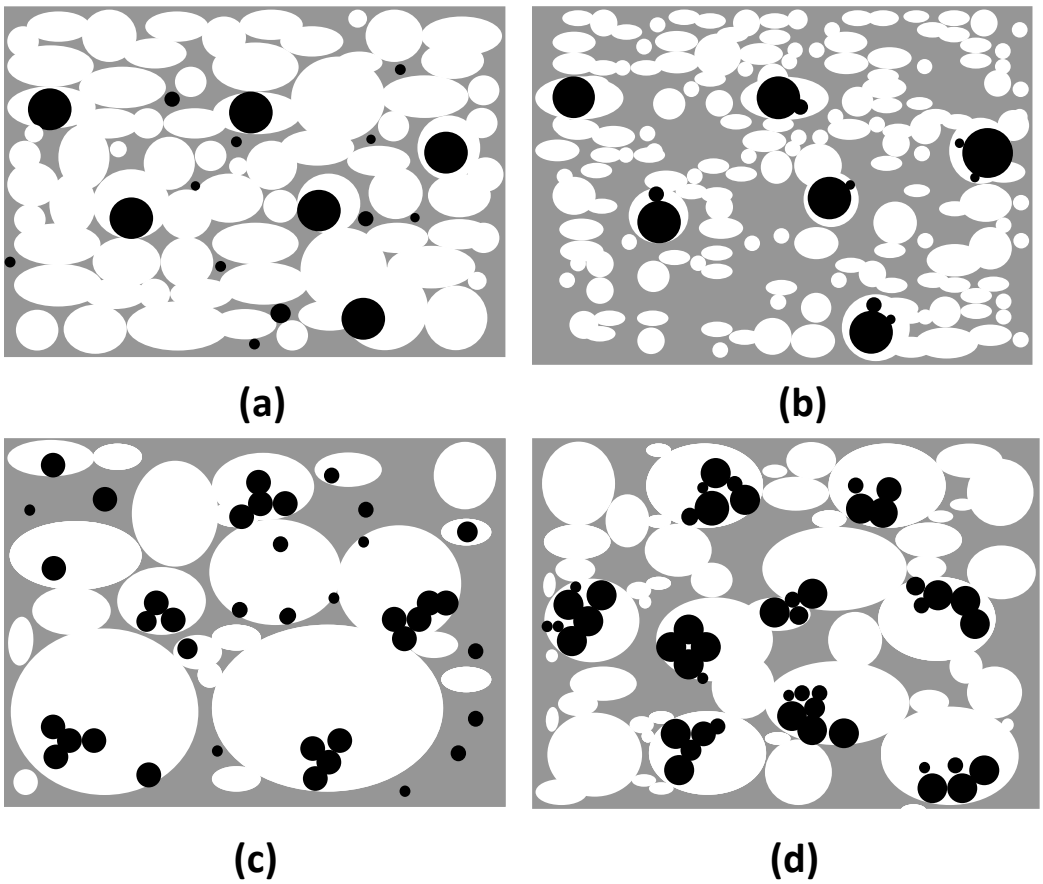

Figure 2. 7 Schematic illustrations of silver particles (black features) and pore size (white regions) of the sol-gel derived silica matrix (gray regions) after calcination for 2 hours at 200°C (a) acid-catalyzed (b) acid/base catalyzed gels, and after calcination for 2 hours at 800°C (c) acid-catalyzed (d) acid/base catalyzed silica gels.

catalysis route leads to larger silver particles/ agglomerates in the silica matrix compared to those formed through acid-catalysis. When the microstructural changes are considered during heating from 200 ºC to 800 ºC; for both processing routes calcination produces densification of the silica leading to relatively smaller pore size after calcination compared to those of the unheated gels. With heat treatment at 800 ºC the acid/base catalyzed silica contains bigger pores; as the initial pore size before heat treatment is considerably larger compared to the acid-catalyzed gel. In addition to above-mentioned microstructural differences as depicted by the schematics in Fig. 5 , another unique property of the acid/base catalyzed gel is the change in silver particle size with calcination temperature. The remarkable character of the acid/base catalyzed

gels is the growth of silver agglomerates with increasing calcination temperature. As the heat treatment temperature increases from 400 ºC to 800 ºC, the silver colloid size increases from approximately 19 ± 2 nm to 32 ± 2 nm. Similar conclusions for silver nanocrystal-doped porous silica films were also previously reported in the literature, suggesting dissolution or partial oxidation of dispersed silver nanocrystals with an average size of 15 nm or smaller during calcination in temperature range of 450 ºC–500 ºC [19]. After further calcination at temperatures higher than 550 ºC coarsening of bigger silver clusters was reported in expense of dissolution of smaller clusters of silver. The similar increase in silver particle size is observed in our study. This increase can be explained by the fact that the dispersed silver nanoparticles in the silica matrix melt to reduce the interfacial energy by Raleigh shape instability; in this way isolated silver particles diffuse to previously formed larger silver particles—agglomerates—on the pore surfaces.

For the acid-catalyzed gels with $[AgNO_3]/[TEOS] = 0.015$ silver particle size is only available for the samples heat treated at 800 ºC (24 nm ± 2), considerably smaller compared to that for acid/base catalyzed gels of the same concentration which have a silver particle size of 32 ± 2 nm. But for the gel with $[AgNO_3]/[TEOS] = 0.060$, the silver sizes were found to be 28 ± 2 and 30 ± 2 nm after 600 ºC and 800 ºC, respectively, suggesting that the silver particle size is not greatly influenced by calcination temperature for this route in the temperature range studied. The silver growth mechanism suggested for acid/base catalyzed gels is also valid for acid-catalyzed system. But, since the initial pore size is smaller and since it gets much smaller with calcination, there is more confined space for the growth of silver agglomerates.

The difference in microstructure of acid and acid/base catalyzed gels significantly affected the resultant antibacterial performance. The acid/base catalyzed silca gels, which have more open microstructure exhibited higher antibacterial activity, compared to acid catalyzed ones. The improvement in antibacterial property in acid/base catalyzed silica gels has been attributed to its open microstructure, which enhance the release of

Ag^+ upon interaction with bacteria cell.

In summary, based on the experimental findings and suggested model, for the acid-catalyzed slow-gelling system; (1) the silica matrix is more dense, with a pore size of less than 25 Å , (2) silver colloids are distributed in a threedimensional silicate network as well as on the pore surface, (3) silver particle size does not change significantly with increasing calcination temperature and (4) has a representative homogenous silver particle size of at around 24–30 nm in the thermal treatment range of 200 ºC– 800 ºC. On the other hand, for the two-step acid/base catalyzed silica; (1) the silica-based matrix exhibit relatively more open microstructure with bigger pores (250 Å), (2) exhibits both isolated dispersed colloidal nanoparticles together with clusters/agglomerates of silver precipitates on the pore surfaces, (3) the size distribution of silver particles changes with calcination temperature; at lower temperatures at around 400 ºC silver is distributed in the silica matrix mostly as dispersed nanoparticles and limited agglomerates of silver colloids with an average size of 19 ± 2 nm yet reach 32 ± 2 nm after a heat treatment of 800 ºC. In addition, with an increase in calcination temperature the number of this isolated colloids decrease as agglomerates grow. This special arrangement of relatively larger silver particles, which act as individual crystallization centers, provides a higher potential for silica crystallization even though silica matrix exhibits more open structure.

2.6 Conclusions

Silica powders incorporated with metallic silver nanoparticles were prepared by two different sol-gel routes. In the first route, slow gelling samples were prepared using organo silicate based aqueous solutions with acid catalyst, while in the second route rapid gelling samples were prepared using a two-step acid/base catalysis. The synthesis method affected both the physical and chemical state of silica matrix and the size of metallic silver. Different synthesis route leads to three major differences for silver doped silica: (i) microstructure—acid/base gels typically have more open space which are mesoporous which is analogous to the pH effect on microstructure for silica gels synthesized from silicon alkoxides. (ii) Size and distribution of silver particles - after

calcination at 800 ºC the acid/base gelation route leads to bigger silver nanoparticles/ agglomerates in silica matrix compared to those formed in the acid-catalyzed systems. According to proposed model acid/base catalyzed system consisted of dispersed nano silver particles and clusters/agglomerates of silver particles at calcination temperatures lower than 450 ºC. The possible mechanism for the formation of silver agglomerates at higher calcination temperature is based on the higher potential for precipitation of bigger silver in the mesoporous silica during gelation and improved diffusion of silver through larger pores of the silica matrix during subsequent calcination. (iii) Crystallization of the silica matrix-crystallization of silica at higher calcination temperatures is promoted in the acid/base catalyzed gels despite their higher porosity. This is related to the distribution of silver particles in the silica matrix and to the change of the size and distribution of silver colloids with calcination temperature. By an increase in calcination temperature, the number of dispersed colloids decreases and some disappear at the expense of the growth of big agglomerates. This special arrangement of silver particles helps crystallization of the silica matrix by reducing the kinetic barrier needed for the crystallization of the surrounding glassy silica matrix.

2.7 References

[1] Tanahashi I, Yoshida M, Manabe Y, Tohda T, "Effects of heat-treatment on Ag particle growth and optical-properties in Ag/ SiO_2 glass composite thin films", J. Mater. Res.,10, 362, (1995).

[2] Matsunami N, Hosono H, "Colloid formation effects on depth profile of implanted Ag in SiO_2 glass", Appl. Phys. Lett., 63, 2050, (1993).

[3] Magruder RH, Ozborne DH, Zuhr RA, "Nonlinear-optical properties of nanometer dimension AG-Cu particles in silica fromed by sequential ion ımplantation", J. of Non-Cryst. Solilds, 176, 299, (1994).

[4] Ahmed AA, Allah E., "Origin of absorption-bands observed in the spectra of silver ion-exchanged soda-lime-silica glass", J. Am. Ceram. Soc., 78, 2777, (1995).

[5] Magudapathy P, Gangopadhyay P, Panigrahi BK, Nair KGM, Dhara S, "Electrical transport studies of Ag nanoclusters embeded in glass matrix", Physica B, 299, 142, (2001).

[6] Brusilovsky D, Eyal M, Reisfekd R, "Absorption spectra, energy dispersive analysis of X-ray and transmission electron microscopy of silver particles in sol–gel glass films", Chem. Phys. Lett., 9, 203, (1988).

[7] Hinsch, A. Zastrow, V. Wittwer, "Sol-gel glasses: A new material for solar fluorescent planar concentrators?", Solar Energy Mats., 21, 151, (1990).

[8] Mennig M, Spanhel J, Schmidt H, Betzholz S, "Photoinduced formation of silver colloids in a borosilicate sol-gel system", J. Non-Crys. Solids, 147, 326, (1992).

[9] Mennig M, Endres K, Schmitt M, Schmidt H. "Colored coatings on eye glass lenses by noble metal colloids", J. Non-Crys. Solids, 218, 373 (1997).

[10] De G, Licciulli A, Massaro C, Tapfer L, Catalano M, Battaglin G, Meneghini C, Mazzoldi P, "Silver nanocrystals in silica by sol–gel processing", J. Non-Crys. Solids, 194, 225, (1996).

[11] Kawashita M, Tsuneyama S, Miyaji F, Kokubo T, Kozuka H, Yamamoto K, "Antibacterial silver-containing silica glass prepared by sol–gel method", Biomaterials, 21, 393, (2000).

[12] Garnica-Romo MG, González-Hernandez J, Hernández-Landaverde MA, Vorobiev Y, Ruiz F, Martinez JR, "Structure of heat treated sol–gel SiO_2 glasses containing silver", J. Mater. Res., 16, 2007, (2001).

[13] Ameen KB, Rajasekharan T, Rajasekharan MV, "Grain size dependence of physic-optical properties of nanometallic silver in silica aerogel matrix," J. Non-Cryst. Sol., 352, 737-746 (2006).

[14] Satyanarayana N, Xie XG, Rambabu B, "Sol-gel synthesis and characterization of the Ag_2O-SiO_2 system", Mater Sci Eng B72, 7-12 (2000).

[15] Chakrabarti K, Whang CM, "Structural and physical properties of Ag doped poly(dimethylsiloxane) modified silica xerogels", J. Appl. Phys., 90, 6493-6499 (2001).

[16] Cao Y, Dai WL, Deng JF, "The synthesis, characterization and application of Ag-SiO_2-Al_2O_3 sol -gel composites", Mater. Lett., 50, 12-17 (2001).

[17] Suyal G, Menning M, Schmidt H, "Effect of glass substrates on the formation of gold-silver colloids in nanocomposite thin films", J. Sol-gel Sci. Technol., 29, 11-18, (2004).

[18] Wu PW, Dunn B, Doan V, Schwartz BJ, Yablonovitch E, Yamane M, "Controlling the spontaneous precipitation of silver nanoparticles in sol-gel materials", J. Sol-gel Sci. Technol., 19, 249-252 (2000).

[19] De G, Licciulli A, Massaro C, Tapfer L, Catalano M, Battaglin G, Meneghini C, Mazzoldi P, Silver, "Nanocrystals in silica by sol-gel processing", J. Non-Cryst. Sol., 194, 225-234 (1996).

[20] De G, Tapfer L, "Formation of copper and silver nanometer dimension clusters in silica", J. Non-Cryst. Sol., 13, 417-420, (1992).

[21] Jeon HJ, Yi SC, Oh SG, "Preparation and antibacterial effects of Ag–SiO_2 thin films by sol–gel method", Biomaterials , 24, 4921-4928, (2003).

[22] Sakka S, Kozuka H, "Sol-gel preparation of coating films containing noble metal colloids, J. Sol-gel Sci. Technol ,13, 701–705 (1998).

[23] Garcia MA, Garcia- M Heras M, Cano E, Bastidas JM, Villegas MA, Montero E, Llopis J, "Photoluminescence of silver in glassy matrices", J. Appl. Phys., 96, 3737 (2004).

[24] Li W, Seal S, Megan E, Ramsdell J, Scammon K, Lelong G, Lachal L, Richardson KA, "Physical and optical properties of sol-gel nano-silver doped silica film on glass substrate as a function of heat-treatment temperature, J. Appl. Phys., 93, 9553-9561 (2003).

[25] Samuneva B, Dimitriev Y, Dimitrov V, Kashchieva E, Encheva G, "Silica Gels and Gel Glasses Containing Silver and Platinum Metal Particles", J Sol-Gel Sci Technol 13:969-974 (1998)

[26] Kokkoris M, Trapalis CC, Kossionides S, Vlastou R, Nsouli B, Grötzschel R, Spartalis S, Kordas G, Paradellis Th, "RBS and HIRBS studies of nanostructured $AgSiO_2$ sol-gel thin coatings, Nucl. Instrum. Meth. Phys. Res. B, 188, 67-72, (2002).

[27] Cullity BD, Stock SR (2001) Elements of X-ray diffraction. Prentice-Hall, New Jersey, pp 170

[28] Brinker CJ, Scherer GW (1990) Sol-gel science: the physics and chemistry of sol-gel processing, Chapter 5. Academic Press, San Diego

[29] Ortega-Zarzosa G, Martinez JR, "Annealing behavior of silica gel powders modified with silver crystalline aggregates, J. Sol-gel Sci. Technol., 27, 255-262,(2003).

[30] Garnica-Romo MG, González-Hernandez J, Hernández-Landaverde MA, Vorobiev Y, Ruiz F, Martinez JR, "Structure of heat treated sol–gel SiO_2 glasses containing silver, J. Mater. Res., 16, 2007-2012, (2001).

[31] Brinker CJ, Scherer GW, Sol-gel-glass 1. Gelation and gel structure, J. Non-Cryst. Sol., 70, 301-322, (1985).

[32] Garnica-Romo MG, Yañez-Limón JM, González-Hernández J, Ramírez-Bon R, Ramírez-Rosales D., Zamorano-Ulloa R., Tı rado-Guerra S., "Structure and electron spin resonance of annealed sol-gel glasses containing Ag, J. Sol-gel Sci. Technol, 24, 105-112, (2002).

CHAPTER 3

EFFECT of CALCINATION on MICROSTRUCTURE and ANTIBACTERIAL ACTIVITY of SILVER-CONTAINING SILICA COATINGS

3.1 Introduction

Silver nanoparticle-embedded glasses or composites have been proposed for various applications such as colored glasses [1, 2], catalysts [3, 4], sensors [5], and substrates for surfaceenhanced Raman spectroscopy (SERS) [6,7]. Silver-incorporated glassy materials are also promising candidates as antibacterial material evident by the available literature [8–10]. Silver containing coatings have been applied onto implant materials such as bioglass [11–13], bone cement [14], dental materials [15], and ceramic orthopedic implant [16–18] to achieve antibacterial activity and to reduce the incidence of postoperative infection**.**

Among various biocides, silver has been long known as an effective antibacterial agent [19,20]. Several studies explain the inhibitory effect of silver against bacteria. It is generally believed that silver in the ionic state associates with the functional groups of enzymes on the bacterial cell wall and inactivating cellular activities such as nutrition and replication and leading to termination of the bacteria [21, 22]. Silver is also effective on a broad spectrum of bacterial organisms. Thus, one frequently used approach to prepare antibacterial materials is to incorporate silver in various polymer or inorganic matrices. In this respect, silver-embedded silica powders or coatings offer unique merits compared to their organic counterparts due their high chemical and

environmental durability, heat resistance, and long-term high antibacterial activity.

Alternative to some other processing techniques such as melt quenching, ion implantation, sputtering, and ion exchange, one easy way of preparing silver-introduced coatings on glass or silica substrates is the sol–gel route. This can be achieved by dissolving silver salts in the sol and subsequent reduction of Ag^{+} to metallic particles by using a reducing agent [23, 24], UV or gamma rays [25, 26], or by thermal treatment in reducing atmosphere [27–29]. For sol–gel-derived silver nanoparticle containing silica coatings, most work has been dedicated on exploring of metallic silver formation mechanism during thermal densification, while the number of investigations on direct correlation of antibacterial activity with structural and chemical changes of the coating surface due to thermal treatment is yet quite limited [9, 30].

In the present study, we report preparation of silver containing silica coatings by sol–gel method on soda-lime glass substrates for use in antibacterial applications. The sol–gel processing of such coatings on glass surface can be adapted for forming antibacterial coatings on different materials such as bioglass, calcium phosphates, dental porcelain/ glass-ceramics, and titanium alloys which have been used in the biomedical field as implant material. The surfaces of these implant materials can be chemically activated for deposition of the coating sols in similar way as activating a glass surface, by introducing (-OH) surface functionalities needed for molecular adhesion of aqueous silica sols with the substrate. The general objective of this study is to establish processing parameters for achieving complete and uniform coating coverage on glass. The effects of drying conditions and postcoating calcination treatment on formation and microstructure of the coatings have been investigated in detail. Special emphasis is given to identify the correlation between the calcination treatment and physical/chemical state of the coating and silver using surface-sensitive analytical techniques such as X-ray photoelectron spectroscopy (XPS) and atomic force microscope (AFM). Another specific objective was to determine the changes in antibacterial activity as a result of structural and chemical changes of the coating surface with calcination.

3.2 Materials and methods

3.2.1 Processing/preparation of coatings

Coating solutions consisted of tetraethyl orthosilicate [TEOS, $Si(OC_2H_5)_4$, Aldrich], silver nitrate ($AgNO_3$, Aldrich), ethanol (C_2H_5OH, Merck), DI water, and nitric acid (HNO_3, Merck). The molar ratio of TEOS:$AgNO_3$:C_2H_5OH:H_2O:HNO_3 was 1:0.015:2:8:0.015. Two solutions were mixed to prepare the final coating solution. First, 0.14 g $AgNO_3$ was dissolved in 5.60 mL DI water and then 0.4 mL of 0.1 M HNO_3 and 2 mL ethanol were added to this solution. The solution was stirred for 20 min. The second solution was prepared by dissolving 9 mL of TEOS in 2.7 mL ethanol by stirring for 20 min. Then the first solution was slowly added into the TEOS–ethanol solution under stirring and final aqueous mixture was further stirred for 100 min at 25ºC. The pH value was recorded as 2.5. The clear aqueous sol was left to age for 3 days prior to coating.

Coating was carried out by using a spin coater (Laurell WS-400B-6NPP-LITE). Soda-lime–silica glass (Gold Seal) microslides were used as the substrate. Prior to coating process the glass slides were subjected to cleaning pretreatment. Glass microslides were first immersed into 0.1 M NaOH at 70ºC and then 0.1 M HCl solutions for 15 min. Rinsing with DI water was performed between these steps and glass pieces were then dried by nitrogen blowing. Following cleaning treatment glass slides were cut into 2.5 X 2.5 cm^2 size pieces. For each spinning application, 1 mL of coating solution was deposited on the precleaned glass substrate with the help of disposable transfer pipette. Coatings were formed by a two-step spinning operation; initially, the spin rate was 2300 rpm for a time span of 55 s, and then the spin rate was decreased to 750 rpm for the following 30 s. After spin coating the samples were dried either in air at room temperature for 6 h or by 1.5 min warm air blowing at 70ºC. In some cases multiple coating processes were applied and same drying treatment was conducted inbetween the subsequent coating steps. After performing all the coating operations and achieving initial drying (70ºC) after each step, transparent and light brown coatings were obtained

and this condition will be referred as ‘‘as-deposited’’ condition for the coatings. Additionally, the coatings were also exposed to a final drying treatment in air at 100ºC for 1 h. This fully dried condition prior to calcination process will be referred as ‘‘as-prepared’’ condition hereafter. Additionally, some samples were calcined in air at 300, 500, and 700ºC for 2 h following 100ºC-drying treatment. Calcined samples were cooled to room temperature by natural cooling in the furnace.

3.2.2 Materials characterization

X-ray diffraction analyses of the samples were performed using a Rigaku D/Max-2000 PC X-ray diffractometer. X-ray source was Ni-filtered CuKa radiation. The X-ray source operating voltage was 40 kV and the scan rate was 2º/min.

The examination of the coating morphology and coverage was performed by using JSM-6400 model SEM operated at 20 kV. Energy dispersive X-ray (EDX) spectroscopy analyses were performed for qualitative chemical identification. All EDX spectra were obtained from a selected area at a magnification of 50X at the center of the samples. EDX analyses of the films were recorded between 0 and 10 keV range.

The optical absorbance of the film products was recorded in the wavelength range of 300–800 nm using an ultraviolet–visible diffusive reflection spectrometer (Varian Bio 100). The background contribution was evaluated by using a precleaned glass microslide.

The surface compositions of coatings were analyzed with a SPECS ESCA X-ray photoelectron spectrometer with Mg/Al dual anode system employing MgKa at 20 mA anode current with an electron-accelerating voltage of 10 kV with a pass energy of 48 eV and a step size of 0.2 eV. Quantitative surface compositions were determined for all samples from high resolution scans of the O 1s, Si 2p, Na KLL, Ca 2p, and Ag 3d spectral regions. Elemental sensitivity factors used for quantification were determined with the use of internal standards and atomic composition estimated using SpecsLab

software. The binding energy was referenced to the C 1s line at 284.5 eV and charge corrections were performed accordingly.

Coating surfaces were imaged, and height, amplitude, and phase-mode images were obtained with a Veeco Nanoscope V atomic force microscope in Tapping Mode using a silicon-sharpened tip (nominal tip radius of 5–10 nm) at a scan rate of 1 Hz. Multiple scans of sizes 1 X 1 μm^2 and 250 X 250 nm^2 were collected at different locations on the surface to ensure representative images.

3.2.3 Antibacterial activity measurements

The antibacterial activity of the coatings was measured by the disk diffusion assay method, and gram-positive bacteria Staphylococcus aureus (ATCC 25923, during preparation of test culture. The second agar, a Muller-Hinton agar (Merck), was used as a seeding environment of the bacteria culture during the long-term exposure of coated samples with bacteria. For preparation of the agar plate, first 40 g agar and 1 L of DI water were mixed to obtain homogenous solution and it was kept at 120ºC and 3 atm pressure for 30 min in autoclave. Following autoclave treatment, solution containing agar colloids was cooled to 50ºC. Then, agar–DI water solution was poured into sterilized polystyrene petri dishes and the mixture was kept at 4ºC in a refrigerator after holding it at room temperature for 2–3 h. The second task in the antibacterial test was the preparation of bacteria culture. Bacteria which had been frozen at 80ºC was kept at 37ºC for 1 day for colony dissociation. Following this process, the bacteria medium was seeded in petri dishes containing the blood agar. Then, they were incubated at 37ºC for 48 h to support multiplication. The final task for antibacterial testing was to attain a longterm contact with the bacterial colonies and coating of the test samples. For this purpose, bacteria colonies which were initially multiplied in blood agar were transferred on a Muller-Hinton agar by spreading with cultiplast. Then coated glass samples (1.25 X 1.25 cm^2 in size) were put face down on the bacteria-seeded agar plate to generate a definite contact with the bacteria-seeded agar and the coated surface. Uncoated glass substrate and an antibiotic pellet (CIP, Cipoxin) were used as control samples in all

antibacterial tests. After 24 h of incubation at 37ºC the widths of the inhibition zones around the samples were measured and related to antibacterial performance.

3.3 Results

3.3.1 Coating morphology and microstructure

The SEM micrographs in Figure 3.1 exhibit the effect of drying process on film formation behavior and on coating coverage. The films exposed to open air drying

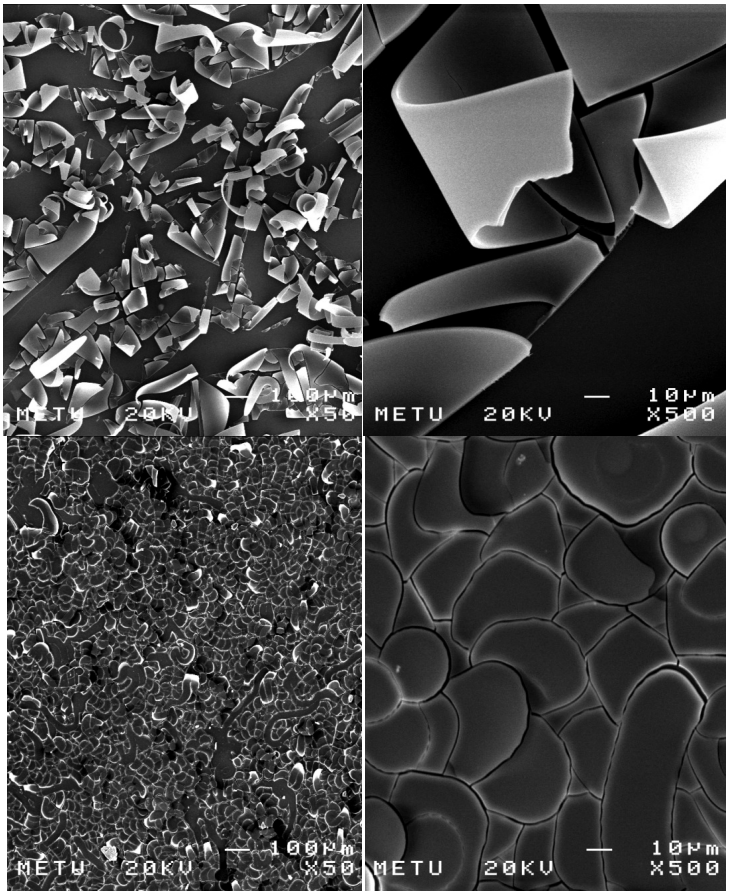

Figure 3.1 SEM micrographs of silver containing silica coatings dried by open air drying at room temperature for 6 h (top) and by warm air blowing at 70ºC (bottom). The images on the right hand side are higher magnification of the same samples shown on the left hand side.

treatment were severely cracked and peeled off from the glass surface. The films formed by warm air drying on the other hand had better coverage/spreading on glass substrate. When deposited as a single layer (~750 nm thick) all films exhibit microcracking to

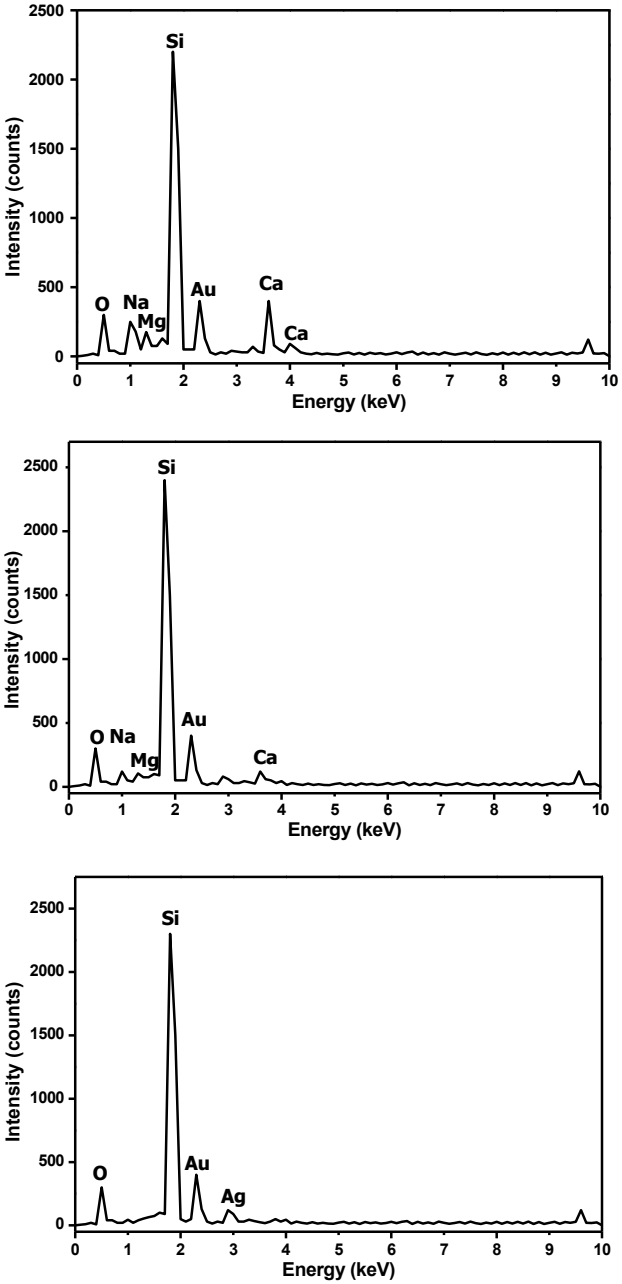

Figure 3.2 EDX spectra of silver-containing silica coatings after calcination at 300ºC produced by (b) single-, (c) two-, (d) three-step coating operation.

some extent controlled by the drying conditions: This problem was more severe in the case of air drying. However, a firm film build up can be achieved for coatings elaborated by multiple coating operations and subsequent warm air drying.

The EDX spectra in Figure 3.2 designate the chemical composition of the coatings and also show how the surface coverage is affected by the number of coating operations. The gold radiation in the spectra is due to the conductive Au-Pd film on the surface of the sample that has been employed to minimize the charging problem during SEM examinations. These representative spectra are for the coatings produced by a single-, two-, and three-step coating operation with identical processing history. If the silica coating is too thin or not completely covering the glass substrate, then the chemical components such as sodium and/or calcium of the underlying glass can contribute to the spectra. In this respect, glass component (sodium and/or calcium) radiations can be considered as an evidence for a thin and cracked coverage by the sol–gel derived silica coating. As can be seen in Figure 3.2(a,b), the EDX spectra of the bare glass and coating formed by single operation are similar. They both contain relatively intense sodium and calcium radiations from underlying substrate indicating poor coverage. However, both calcium and sodium radiations weaken with increasing number of coating applications [Figure 3.2(c)] and completely disappear for the coating obtained by three-step coating operation [Figure 3.2(d)]. This suggests that a more dense and continuous coverage can be achieved more effectively for coatings formed by multiple coating operation. Throughout the rest of this study, the coatings formed by single coating operation will no longer used/considered. The samples obtained by three-step coating operation and warm air drying exhibiting better coverage and minimal crack formation will be referred to as the standard coating. These coatings were further investigated for their microstructural and functional properties. These coatings were further investigated for their microstructural and functional properties.

3.3.2 XRD analyses

Figure 3.3 shows the XRD patterns of the coatings in as-prepared condition and after heat treatment at 300, 500, and 700ºC. For the as-prepared sample only a broad peak representing the amorphous silica network is present. No other peaks for silver or for any other crystalline phases are present. Calcination at 300ºC leads to formation of a new peak located at 2θ= 38º which is for metallic silver (JCPDS card no. 4-0783). The intensity of this silver diffraction peak increases for the samples calcined at 500 and 700ºC. In addition, after heat treatment at 700ºC, the second peak related with metallic silver formation located at 2θ= 45º arises. Sol–gel-derived silica matrix remained amorphous even after heat treatment at 700ºC.

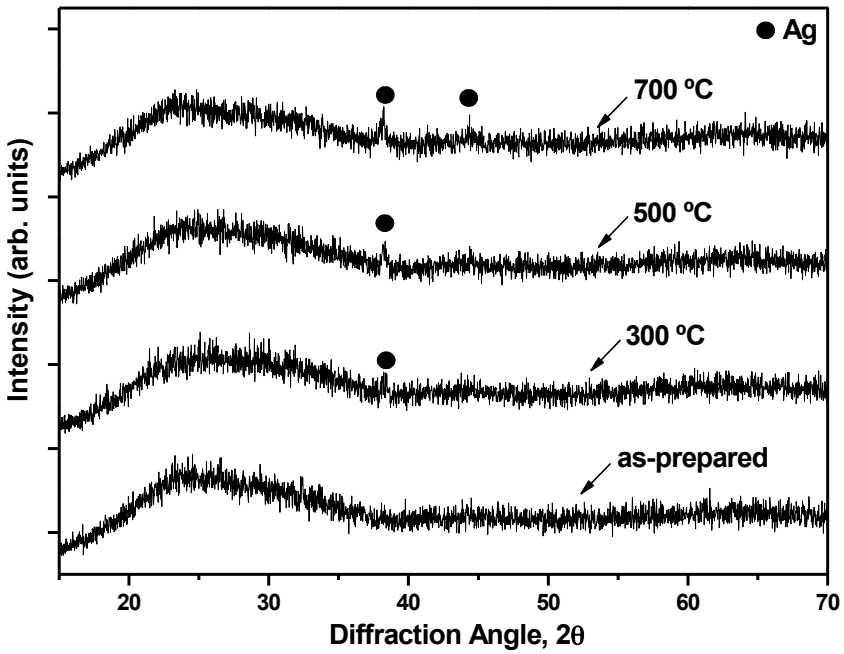

Figure 3.3 X-ray diffraction patterns of silver-containing silica coatings at different processing conditions.

3.3.3 Optical properties

The optical properties of the coatings are shown in Figure 3.4. Figure 3.4 presents the absorption spectra of the samples in as-prepared condition, calcined at 300, 500, and

700ºC. In as-prepared condition the spectra do not reveal a distinct absorption, but display only a very broad band in the visible range. The spectra of the 300ºC-calcined sample exhibit a relatively broad absorption band at 450 nm attributed to the silver particles. This broad band centering at around 450 nm shows a red shift with respect to the surface plasmon resonance (SPR) peak of silver at 412 nm [31–33]. This spectra also consist of a small broad absorption band, which appears as a shoulder at around 350 nm, assigned for the atomic silver clusters [34–36]. Further increase in the calcination temperature to 500ºC leads to disappearance of the small band at 350 nm and to a reduction in the intensity of SPR peak (at 412 nm) of silver. However, after heat treatment at 700ºC, the intensity of SPR peak of silver increased noticeably and it became narrower.

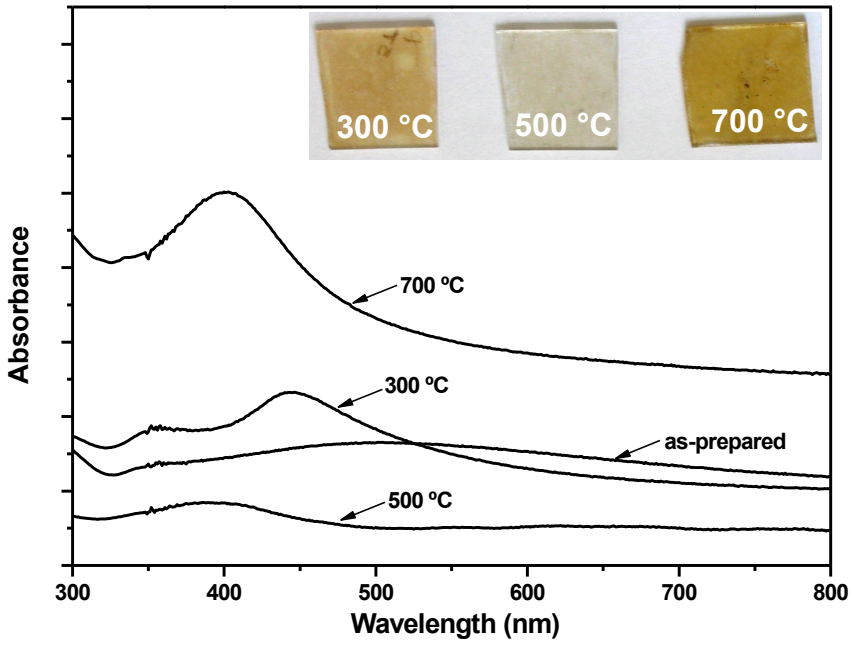

Figure 3.4 UV–vis absorption spectra of silver-containing silica coatings at different processing conditions. The photographs in the inset show the color of the films after calcination at 300, 500, and 700ºC (left to right). Note that the yellow color vanishes for 500ºC-calcined sample.

The physical appearance (color) of the coatings also changes with calcination temperature as shown by the pictures provided as an inset in Figure 3.4. In as-prepared

condition the coatings were light brownish and transparent. The film becomes pale yellow after calcination at 300ºC. After calcination at 500ºC, accompanied by lower SPR absorption band intensity, the yellowish color of the film vanished and the film became clear and almost fully transparent. However, the change in color of the film is reversible and turns back to yellow after calcination at 700ºC.

3.3.4 Surface chemical analyses

XPS analyses of the coatings showed the presence of elements such as adventitious C, Si, O and Ag, Na, Ca in some cases. XPS results are presented in Figures 3.5 and 3.6. Figure 3.5 shows the survey analyses spectra of the coatings in as-deposited and as-prepared conditions and after calcination at different temperatures. The details and important remarks about the survey analyses are emphasized by the regional spectra of selected elements as shown in Figure 3.6. Table 3.1 summarizes the surface chemical

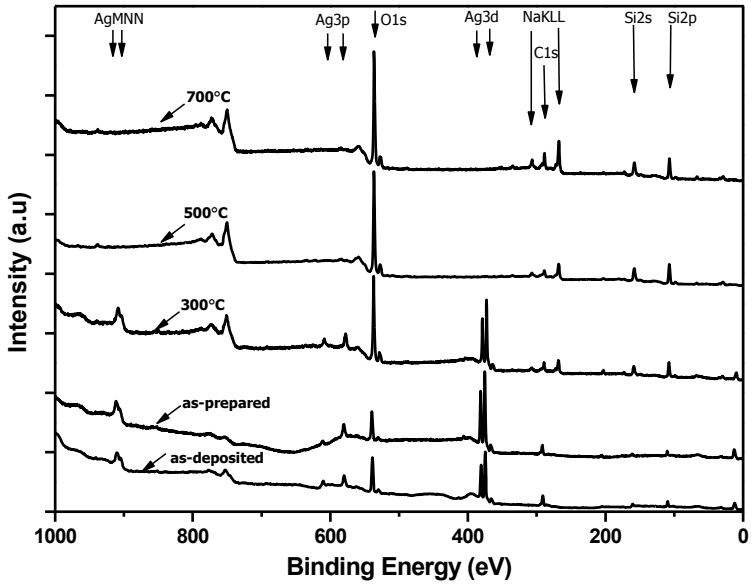

Figure 3.5 Representative XPS survey spectra of the silver-containing silica coatings at different processing conditions. Surface composition differences among the samples are highlighted with the remarks indicating the spectral regions of the major constituent elements.

compositions determined from quantitative analyses of the high resolution regional scans. The influence of calcination temperature on the amount of silver at the coating surface is represented by Figure 3.6(a). Figure 3.6(a) shows the Ag 3d region of the spectra obtained by high resolution scans of the coatings in as-deposited and as-prepared conditions and after calcination at 300, 500, and 700ºC. The peaks centering at around 367.9 and 374 eV are assigned for Ag $3d_{5/2}$ and Ag $3d_{3/2}$, respectively. Silver is present on the film surface for as-deposited, for as-prepared, and for 300ºC-calcined samples. Surface silver content decreases as the heat treatment temperature increases. The intensity of doublet Ag 3d peaks drastically decreases after calcination at 500ºC. No

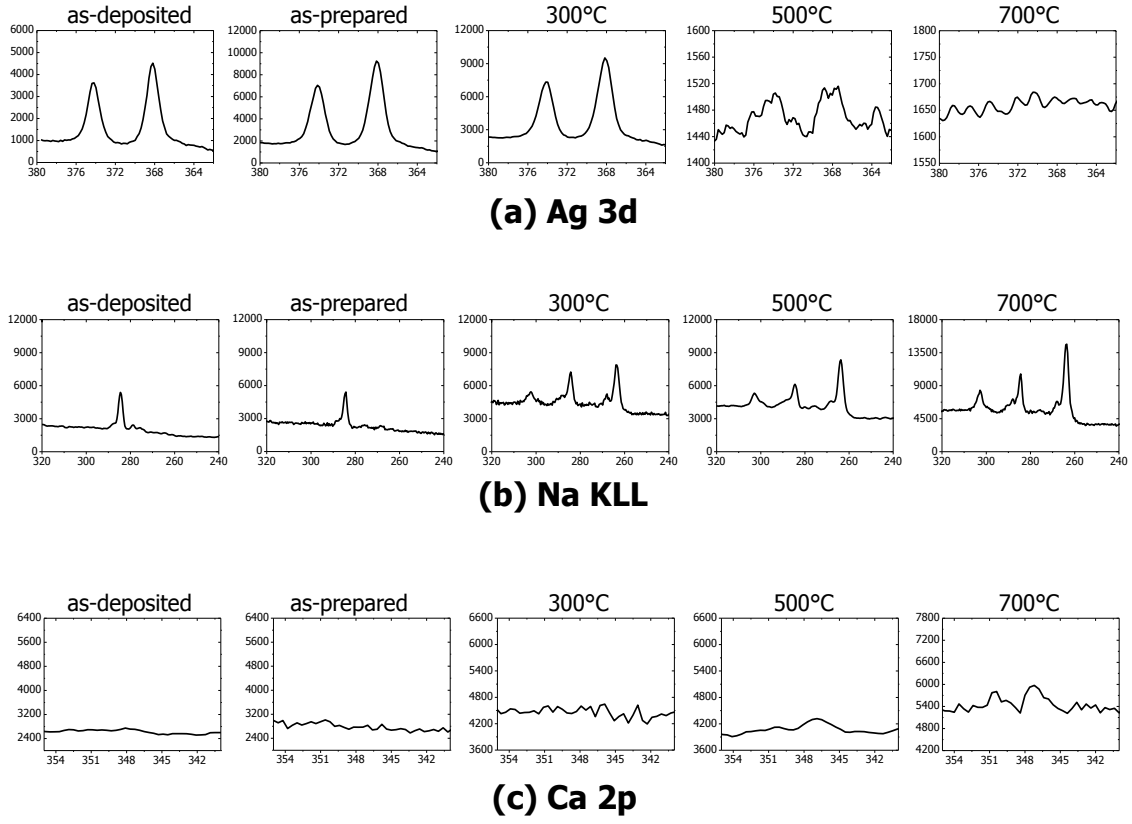

Figure 3.6 High resolution (a) Ag 3d, (b) Na KLL, and (c) Ca 2p spectra of the silver-containing silica coatings at different processing conditions (left to right: as-deposited, as-prepared, and after calcination at 300, 500, and 700ºC). In all graphs, x-axes are binding energy (in eV) and y-axes are intensity (in counts). Note the interdiffusion of Ag and glass components Na and Ca with increasing calcination temperature.

silver peak was detected for the sample calcined at 700ºC. In as-deposited condition, the silver amount on the surface was found as 8.9 at.% and it decreased to 7.1, 6.8, and 0.1 at.% after heat treatment at 100, 300, and 500ºC, respectively. On the other hand, higher calcination temperature resulted in a gradual increase in sodium and calcium amount. In as-deposited and as-prepared conditions, no sodium or calcium peak was observed as shown in Figure 3.6(b). Heat treatment at 300ºC leads to appearance of the sodium (KLL) peaks. Sodium content (in at.%) for this temperature was found as 13.3 and it

Table 3.1 Approximate surface chemical composition of the silver-containing silica coatings at different processing conditions as determined by XPS

SAMPLE	C (at.%)	Si (at.%)	O (at.%)	Na (at.%)	Ag (at.%)	Ca (at.%)	O/ Si	Na/Si	Ag/Si	Ca/Si
as-deposited	30.3	15.1	50.7	-	8.9	-	3.35	0	0.60	0
as-prepared	29.2	12.4	44.6	-	7.1	-	3.60	0	0.57	0
calcined at 300°C	14.7	15.0	48.8	13.3	6.8	-	3.25	0.88	0.45	0
calcined at 500°C	11.1	17.5	53.1	16.7	0.1	0.3	3.03	0.95	0.006	0.017
calcined at 700°C	19.2	14.4	47.0	19	-	0. 4	3.26	1.32	0	0.028

increased to 16.7 then to 19.0 after heat treatment at 500 and 700ºC, respectively. Calcium peaks (2p) in the XPS high resolution scans similarly were detected for 500ºCand 700ºC-calcined samples [Figure 3.6(c)]. Calcium amount (in at.%) for the sample calcined at 500ºC was found as 0.3 and it increased to 0.4 after heat treatment at 700ºC.

The change in the chemical state of silver as a function of calcination temperature was also determined from the variations in binding energies. The binding energy and position of Ag 3d peaks change with calcination temperature. Table 3.2 presents the doublet Ag 3d peak positions for asdeposited and as-prepared conditions and for calcination treatments at different temperatures. As shown in Table 3.2, the peak position of Ag $3d_{3/2}$ for the as-deposited condition is at 374.22 eV, shifting gradually to lower binding energies with increasing temperature, reaching a value of 374.10 eV for the 500ºC-calcined sample. Similarly, Ag $3d_{5/2}$ peak position is at 368.18 eV for as-deposited films and it changes to 367.98 eV with increase in calcination temperature to

Table 3.2 Binding energies (in eV) for Ag $3d_{3/2}$ and Ag $3d_{5/2}$ for silver-containing silica coatings at different processing conditions

SAMPLE	Ag $3d_{3/2}$	Ag $3d_{5/2}$
as-deposited	374.22	368.18
as-prepared	374.12	368.14
calcined at 300°C	374.13	368.13
calcined at 500°C	374.10	367.98
calcined at 700°C	n.a.	n.a.

500ºC. The binding energy change and related peak position shifts in XPS spectrum suggest that the chemical state of silver changes during thermal treatment.

3.3.5 Surface morphology

Figure 3.7 shows representative images of the coatings surfaces calcined at 300 and 500ºC as observed by tapping-mode AFM studies. Both the height images and phase-mode images are shown in this figure. The general surface morphology as examined by height-mode images reflects the three-dimensional appearance of the sol–gel-derived silica coating, which does not change with calcination temperature as the height images follow similar topographical features. The phase image data on the other hand exhibits a clear distinction. AFM phase mode can facilitate comparison of two surfaces where mechanical contrast can be obtained between glassy silica and silver regions. The phase lag reflects the differences in stiffness between metallic silver and glassy silica phases, providing a qualitative mapping of the mechanical properties of the surface. Randomly dispersed bright spots with an approximate average size of 3–35 nm for the 300ºC calcined surface are also representative for as-prepared condition. These spots are comparably smaller for 500ºC-calcined sample with an approximate size in the range of 2–5 nm and cover a smaller portion of the surface compared to that for the 300ºC-calcined surface. These bright spots in the phase-mode AFM images are due to the localized differences in mechanical interaction between the tip and the surface

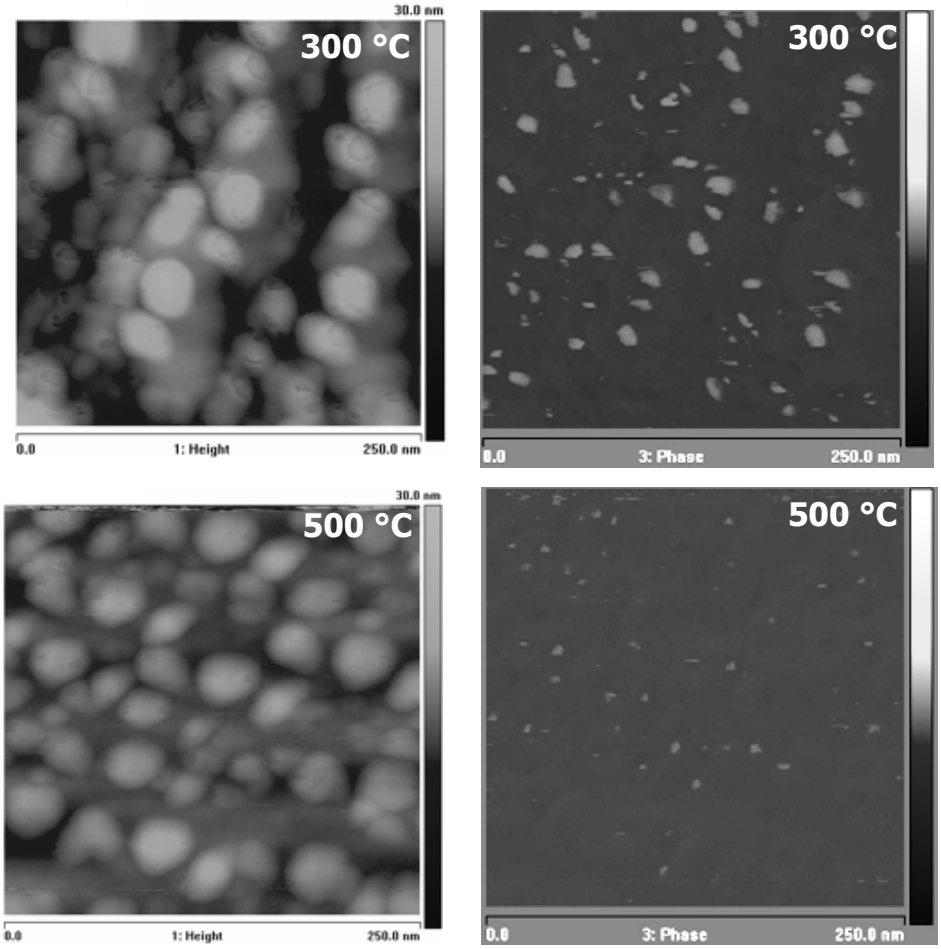

Figure 3.7 AFM imaging of silver-containing silica coatings calcined at 300 and 500ºC under two tapping modes, height (left) and phase lag (right). The height scale light to dark is 30 nm. The phase lag reflects the differences in stiffness between silver and silica phases, providing a qualitative mapping of the mechanical properties of the surface.

originating from chemical variation. In that respect, the phase-mode images provide information about the presence and distribution of silver particles implanted on the surface of the silica matrix. AFM analyses suggest that the silver particles located on the surface disappear with increasing calcination temperature.

3.3.6 Antibacterial activity

Antibacterial performance of coatings as a function of calcination temperature and number of coating operations were assessed by the disk diffusion assay against Staphylococcus aureus. The optical camera pictures in Figure 3.8 show the effect of calcination temperature on antibacterial performance of the standard coating formed by three subsequent coating operations. These pictures show the interaction of the coating surface and bacteria containing agar after 24 h. The white linear marks in these pictures are the bacterial colonies in/on the agar. Antibacterial activity was assessed from the changes in the regions bordering between the coated samples and bacteria-seeded agar. The presence and the size of the dark region around the sample free of linear formations is the inhibition zone (reflecting the antibacterial activity). The as-prepared sample dried at 100ºC clearly shows a remarkable antibacterial activity and the bacterial growth-free, 3–4 mm wide, inhibition zone can be clearly seen around this sample. However, the antibacterial activity gradually weakens with increasing calcination temperature. After heat treatment at 300ºC, the size of the inhibition zone of the coating formed by three coating operations decreases to a value less than 1 mm. For the samples calcined at 500 and 700ºC, no clear inhibitory zone was observed and bacterial growth occurred on/around the coated surface (coatings did not show antimicrobial activity).

Antibacterial activity was also revealed by the visual changes on the surface of the sample which makes contact with the agar surface. The clear/transparent appearance of as-prepared and 300ºC-calcined samples as shown by Figure 3.8(b,c) also implies effective termination of the bacterial growth for these samples. The sample surfaces appear hazy for the coatings calcined at 500 and 700ºC due to deficient antibacterial action. Figure 3.9 shows the effect of number of coating operations on antibacterial activity, where the representative antibacterial activity test photographs of the 300ºC-calcined coatings produced by a single-, three-, and five-step coating operation are shown. It is obvious that the antibacterial activity has improved greatly with increasing the number of coating layers. As shown in Figure 3.9 the antibacterial activity of the coatings obtained by five-step coating process with wider inhibition zones is superior

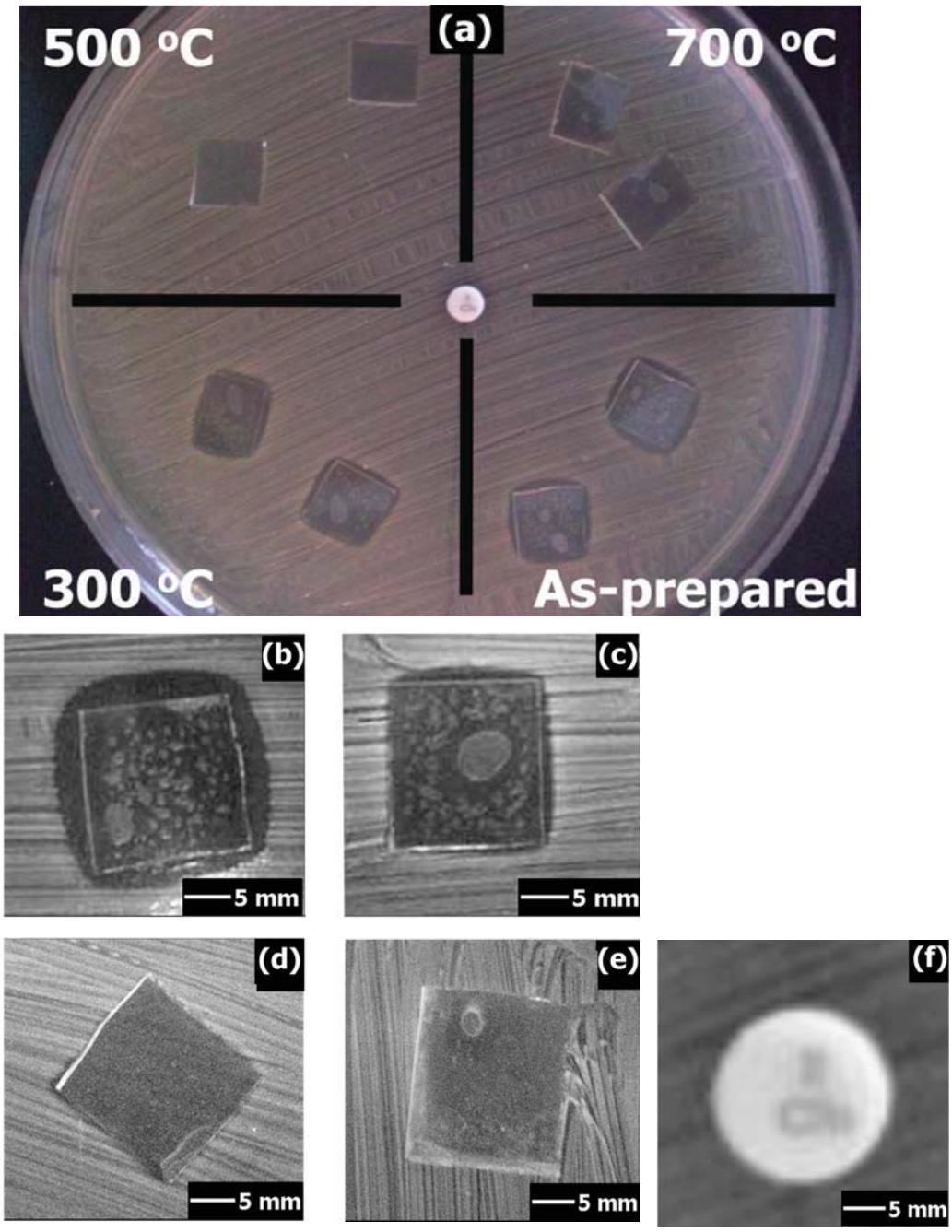

Figure 3.8 Photographs of antibacterial test results against Staphylococcus aureus after 24 h showing the antibacterial activity of the coatings. Top picture (a) shows examples of contact tests performed on agar plate and representative higher magnification views for each sample are shown; (b) in as-prepared condition, after calcination at (c) 300ºC, (d) 500ºC, (e) 700ºC, and (f) antibiotic (CIP, Cipoxin) pellet used as control sample.

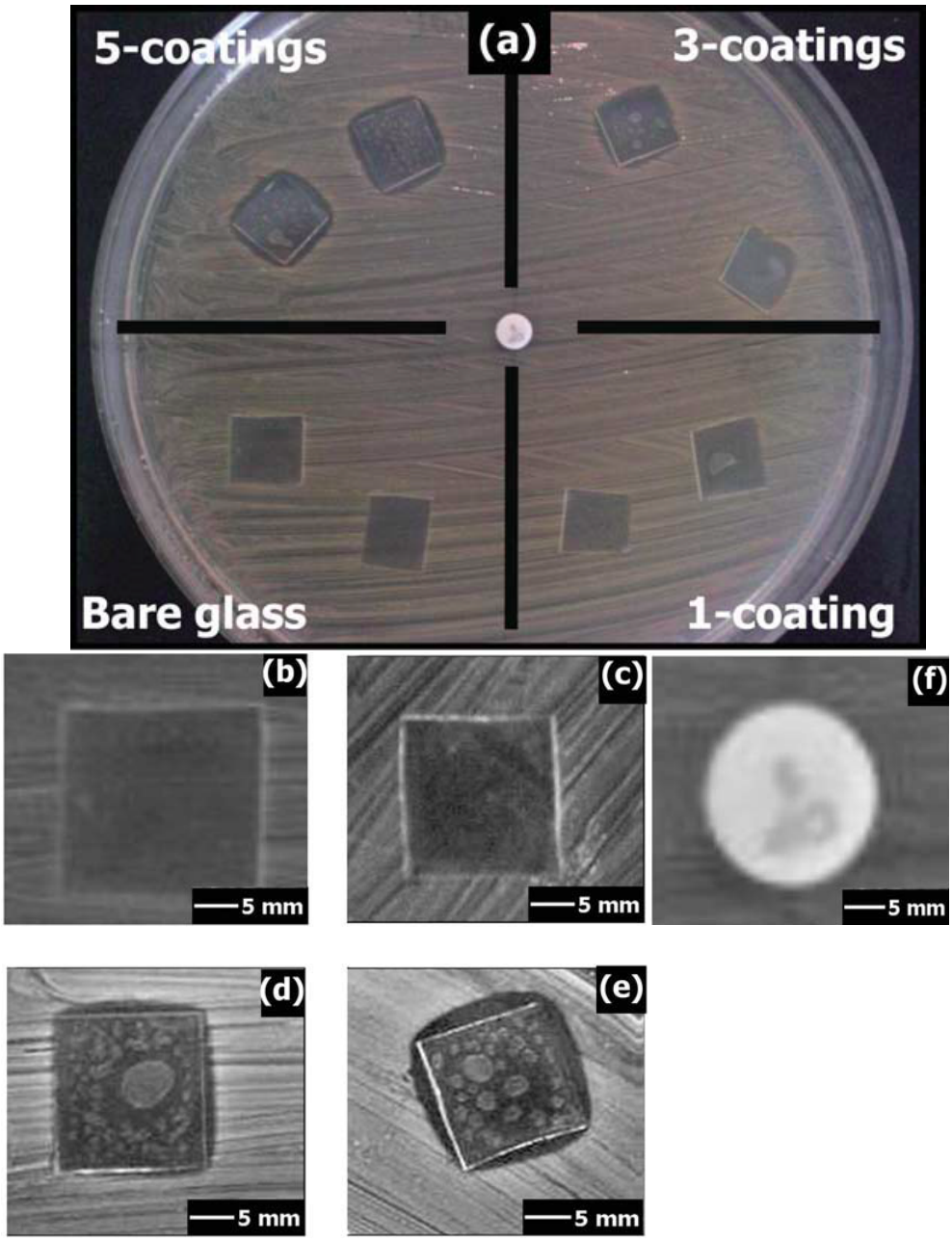

Figure 3.9 Photographs of antibacterial test results against Staphylococcus aureus after 24 h showing the antibacterial activity of the 300ºC-calcined coatings produced by different number of coating operations. Top picture (a) shows examples of contact tests performed on agar plate and representative higher magnification views of each sample are shown; (b) bare glass, (c) single-, (d) three-, (e) five-step coating operation, and (f) antibiotic (CIP, Cipoxin) pellet used as control sample.

compared to coatings produced by a single- and three-step coating operations.

3.4 Discussion

A number of processing parameters are critical in obtaining silver-containing silica coatings on soda-lime–silica glass. As revealed by SEM and accompanying EDX analyses, better surface coverage can be obtained by multiple coating applications and optimization of the drying conditions of the silicon alkoxide-based aqueous sol. Open air drying at room temperature resulted in peeling off the coating from the substrate surface. On the other hand, the films prepared under warm air drying showed better coverage properties without any flaking. Although the mechanism is not clear, open air drying treatment at room temperature for 6 h leads to complete evaporation of liquids such as ethanol and water from the film surface leading to intensive surface tension during drying. The increase in surface tension, which is not balanced with capillary forces, leads to formation of cracks and lift off of the film during long-term drying under ambient conditions. Films dried under warm air blowing treatment at 70ºC with much shorter drying times stay in semigel state with limited liquid evaporation after each drying treatment, keeping contact with the substrate and enabling application of the subsequent coating layer.

For the sol–gel-derived coatings, a series of analytical characterization techniques provided insights about the formation of silver, as well as its size, chemical state, distribution, and location within the silica matrix as a function of calcination temperature. These factors eventually define the overall surface chemical properties that essentially control the antibacterial activity. The presence of silver colloids in the silica matrix for calcined samples was confirmed initially by XRD analyses. In the as-prepared state (dried 100ºC), coatings are completely amorphous. On the other hand, the diffractograms of calcined samples treated at 300ºC or higher temperatures
exhibited peaks for metallic silver together with broad amorphous peak of silica.

The presence of silver colloids after calcination was also recognized by UV–vis

spectroscopy (surface plasmon absorption peaks) as well as by surface chemical analyses with XPS. XPS data confirmed presence of silver even in as-prepared condition. The absence of silver XRD peak for coatings in as-prepared condition may be due to the intrinsic limitation of XRD for phase detection or due to limited formation of silver colloids in amorphous silica matrix, because the broad peak for amorphous silica overlaps with the most intense diffraction peak of silver, which is in trace amount for detection by XRD. Another critical observation from XRD analyses is the increase in the intensity of the silver diffraction at higher calcination temperatures. Thermally induced metallic silver colloid formation during preparation of silver nitrate containing aqueous silica organic sols had been reported by other investigators [35, 37]. The silver nitrate in the sol decomposes to silver and nitrate ions; during calcination, the nitrate ions were expelled in the form of nitrogen gas and thermally promoting spontaneous reduction of silver ions. There are various explanations for the reduction mechanism of silver ions into metallic form. The reduction to metallic silver in the coatings can also occur by cation exchange process between Ag^{+} and hydrolyzed silica sol (Si-OH) leading to an autoreduction as suggested by various investigators [35, 38–40] or by a spontaneous reduction from alcohol radicals that generate during hydrolysis and condensation [41].

The optical absorption data of the sol–gel-derived coatings calcined at different temperatures show the effect of calcination temperature on silver colloid formation extent in silica films. Additionally, the spectral positions of surface plasmon peaks can be interpreted and related to the size and distribution of the silver colloids effectively changing with calcination temperature. Fully dried (at 100ºC) sample does not exhibit a well-defined absorption band that can be assigned to colloidal silver. For the films calcined at 300ºC, UV–vis spectra revealed broad surface plasmon resonance (SPR) absorption at around 450 nm and another absorption band at low wavelength at around 350 nm. The broadening of the SPR peak implies a size distribution for silver particles. The presence of the additional low wavelength band also suggests presence of metallic silver in different sizes. This additional band is assigned to atomic silver clusters which are smaller than silver colloids dispersed in silica matrix [34, 35]. The appearance of

this low wavelength band can also be attributed to the morphology of silver particles associated with presence of oblate spheroid particles [42–44]. In our case, the former possibility is thought to be the reason, because the low wavelength absorption band disappears after calcination at 500ºC. However, for 500ºC-calcined coating, the absorption band due to surface plasmon resonance of silver nanoparticles remains, suggesting elimination of atomic silver clusters by aggregation into larger silver particles or undergoing some other chemical/physical change upon calcination at 500ºC.

The effect of increasing calcination temperature is different on the silver entities with different sizes. For the silver colloids, the blue shift in the peak position after calcination at 500ºC is associated with a narrower size distribution. Further increase in calcination temperature to 700ºC resulted in higher intensity and relatively smaller full width at half maximum (FWHM) of the SPR absorption band located at around 412 nm of stable silver colloids. Both intensity increase and spectral position changes are indicative of an increase in size of silver particles by diffusion-controlled coalescence, as originally suggested by fundamental work from Kreibig and by some other investigators as explained by mean free path effect [45, 46]. In agreement with our optical analyses and some other works, increasing intensity of the silver diffraction peak during XRD analyses additionally supports growth of colloidal silver particles by increasing calcination temperature [46–48].

The second group of silver entities, the atomic silver clusters with much smaller size, undergo chemical change with an increase in calcination temperature. This is revealed by a thermochromic effect, where series coloration and bleaching events occur during calcination in the temperature range studied. A light yellowish color of the silver-containing silica coating calcined at 300ºC is indicative for metallic silver [8, 28, 35]. In our case, the yellow color vanishes after calcination at 500ºC. However, this discoloration effect is reversible, and after calcination at 700ºC, the color again becomes dark yellow. This event has been reported in similar sol–gel systems and has been attributed to aggregation–disaggregation of silver particles [49] or reduction/oxidation of silver [28, 35, 50, 51].

The optical change to transparency for our coatings by calcination in the temperature range 300–500ºC can be explained by size-dependent oxidation of silver in air. Metallic silver is normally stable and does not oxidize in air above 200ºC. However, differences in thermal and structural behavior for nanosized and bulk materials can be excluded. The thermodynamic analyses for oxidation of silver nanoparticles by taking surface energy and curvature effect into account have shown that below a certain critical particle size (at around 3 nm) the oxidation of silver is also possible in air at above 200ºC [52]. Accordingly, at 300ºC, silver exhibits size distribution; however, silver entities are most likely smaller than this critical size. Upon subsequent calcination at 500ºC, these small nanoparticles oxidize giving rise to loss of the coating color. Similar findings on loss of color for silver-containing silica when silver is in ionic form are reported elsewhere.8 In addition, according to XPS analyses conducted in our study, color bleaching seems to be related to oxidation of silver atomic clusters in the temperature higher than 300ºC, parallel to the results of some other investigators [35, 53, 54]. The binding energy of Ag ($3d_{5/2}$) for Ag, AgO, and Ag_2O is determined as 368.2, 367.8, and 367.4 eV, respectively, in the literature [55, 56]. In our case, silver $Ag3d_{5/2}$ binding energies were found as 368.13 and 367.98 eV, for samples calcined at 300 and 500ºC, respectively. Lower binding energies reveal a mixed chemical state for silver which is present both in metallic and oxide form. Relatively lower binding energy for 500ºC-calcined sample also qualitatively suggests that the metallic state concentration is lower compared to the sample calcined at 300ºC. Calcination at 700ºC leads to yellow coating color due to presence of metallic silver particles. It is known that at high temperatures metal oxides are reduced to metals if the kinetic considerations are satisfied, as the redox equilibrium tends to move to reduction side as the temperature rises [57]. Therefore, Ag_xO_y particles, in turn, decompose and form silver nanoparticles in air at temperatures higher than 500ºC, resulting in enhanced SPR intensity.

Besides controlling the size and chemical state of silver, another clear effect of increasing calcination temperature on surface chemical properties is the stimulation of silver nanoparticle diffusion into the bulk of the coatings. XPS analyses clearly show

migration of silver nanoparticles from surface into the bulk. The amount of silver present on the surface of the silica coatings drastically decreases after calcination at 500ºC. Diffusion of silver into the substrate during thermal treatment has also been pointed out by Rutherford backscattering spectroscopy (RBS) analyses by a number of different studies [30, 35]. This most likely occurs by the exchange of silver ions in the coating with sodium ions of underlying glass substrate [53, 58, 59]. The AFM analyses provided here also demonstrated that the silver diffuses into the substrate during calcination. The antibacterial activity was greatly influenced by calcination temperature-dependent changes in the distribution of surface silver in silica coatings. The best antibacterial performance can be attributed to fully dried sample in as-prepared condition, where both silver clusters and ions are readily available on the surface due to lack of diffusion into bulk of the coating. Coatings still exhibit reasonable antibacterial activity upon calcination up to 300ºC. However, antibacterial performance greatly reduces with increasing calcination temperature (to 500ºC) as silver starts to effectively migrate into deeper positions. For both calcination treatments at 500 and 700ºC, no inhibitory zone was observed and bacterial growth actually occurs on the coated surface. The optical and XRD analyses verify presence of the silver in the coating; therefore, it is possible to conclude that the silver nanoparticles are mostly embedded deep in the silica coating or within the glass substrate after calcination at 500ºC. AFM studies as depicted by phase lag-mode analyses revealing a qualitative mapping of the surface also imply a reduced silver nanoparticle concentration at the surface after calcination at 500ºC.

In summary, calcination treatment is required for densification and integration of the coating with the glass substrate and hence achieving structural stability. However, such thermal treatment at temperatures higher than 300ºC leads to degradation of antibacterial activity promoting interdiffusion of silver accumulated on the surface and alkaline glass components such as sodium and calcium. These aspects need to be further improved for the coatings to be considered for ultimate use; however, the results presented in this study provide some insights on some available solutions and processing strategies for achieving such goal. For example, the loss in antibacterial activity may be prevented to some extent by increasing the thickness of the silver-

containing silica coating limiting the interdiffusion. Silver diffusion can be also minimized by achieving gradient chemical (silver content) and microstructural (microporosity) modifications in layered coatings. Additionally, modified multilayered coatings with silica barrier layer in-between the silvercontaining coating and the glass can also hamper the Ag/Na interdiffusion. These processing modifications might enable use of higher calcination temperatures for improved densification and consequently a realization of higher chemical durability for the coatings.

3.5 Conclusions

Antibacterial silica coatings containing silver nanoparticles were synthesized by sol–gel on soda-lime glass substrates. It has been found that silver nanoparticles can be formed in sol–gel-derived silica coatings, which exhibit a size distribution and remain in close proximity of the surface in as-prepared condition and after calcination at temperatures lower than 300ºC. Increasing calcination temperature leads to oxidation of small silver particles around 500ºC and subsequent reduction to metallic silver at 700ºC, as revealed by reversible optical bleaching and coloration. Thermally stable silver colloids with bigger size continuously grow with increasing calcination temperature. Calcination at temperatures higher than 300ºC also initiates migration of silver from the surface into the bulk of the coating. The change in surface concentration and distribution of the silver by interdiffusion of sodium and calcium from the underlying glass at high calcination temperatures leads to a degradation in the antibacterial activity.

3.6 References

[1] Armistead WH, Stookey SD, “Photochromic silicate glasses sensitized by silver halides”, Science, 144, 150–154 (1964).

[2] Morimoto T, Sanada Y, Tomonaga H, “Wet chemical functional coatings for automotive glasses and cathode ray tubes”, Thin Solid Films, 392, 214–222 (2001).

[3] Murphy CJ, Sau TK, Gole AM, Orendorff CJ, Gao J, Gou L, Hunyadi SE, Li T,

"Anisotropic metal nanoparticles: Synthesis, assembly, and optical applications", Phys Chem, 109, 13857–13870 (2005).

[4] Vaskelis A, Jagminiene A, Tamasauskaite-Tamasiunaite L, Juskenas R, "Silver nanostructured catalyst for modification of dielectrics surface", Electrochim Acta 50:4586–4591 (2005).

[5] Xu J-Z, Zhang Y, Li G-X, Zhu J-J, "An electrochemical biosensor constructed by nanosized silver particles doped sol–gel film", Mater Sci Eng C, 24, 833–836 (2004).

[6] Lee YH, Dai S, Young JP, "Silver-doped sol–gel films as the substrate for surface-enhanced Raman scattering. J Raman Spectrosc", 28:635–639 (1967).

[7] Maruszewski K, Jasiorski M, Hreniak D, Strek W, Hermanowicz K, Heiman K, "Raman spectra of molecules adsorbed on Ag centers in sol–gel matrices., J Sol-Gel Sci Technol, 26:83–88.

[8] Toshikazu T. Antimicrobial agent composed of silica-gel with silver complex. Inorg Mater., 6, 505–511 (1999).

[9] Kawashita M, Tsuneyama S, Miyaji F, Kokubo T, Kozuka H, Yamamoto K, "Antibacterial silver-containing silica glass prepared by sol–gel method", Biomaterials 21, 393–398 (2002).

[10] Jeon H-J, Yi S-C, Oh S-G, "Preparation and antibacterial effects of Ag-SiO_2 thin films by sol–gel method", Biomaterials, 24, 4921–4928 (2003).

[11] Blaker JJ, Nazhat SN, Boccaccini AR, "Development and characterization of silver-doped bioactive glass coated sutures for tissue engineering and wound healing applications, "Biomaterials, 25, 319–1329 (2004)

[12] Masuda N, Kawashita M, Kokubo T, "Antibacterial activity of silver doped silica glass microspheres prepared by a sol–gel method.", J Biomed Mater Res B Appl Biomater, 83:114–120, (2007).

[13] Raucci MG, Adesanya K, Silvio LD, Catauro M, Ambrosio L, "The biocompatibility of silver-containing Na_2O-CaO-$2SiO_2$ glass prepared by sol–gel method: In vitro studies, "J Biomed Mater Res B Appl Biomater., 92, 102-110 (2010).

[14] Alt V, Bechert T, Steinru¨ cke P, Wagener M, Seidel P, Dingeldein E, "An in vitro assessment of the antibacterial properties and cytotoxicity of nanoparticulate silver bone cement" Biomaterials, 25:4383–4391 (2004)

[15] Cinar C, Ulusu T, Ozcelik B, Karamuftuogluoglu N, Yucel H, "Antibacterial effect of silver-zeolite containing root-canal filling material, J Biomed Mater Res B Appl Biomater, 90, 592–595 (2009).

[16] Chen Y, Zheng X, Xie Y, Ding C, Ruan H, Fan C, "Antibacterial and cytotoxic properties of plasma sprayed silver-containing HA coatings", J Mater Sci Mater Med.,19, 3603–3609 (2008).

[17] Li B, Liu X, Cao C, Dong Y, Ding C, "Biological and antibacterial properties of plasma sprayed wollastonite/silver coatings", J. Biomed. Mater Res. B Appl. Biomater. 91, 596–603 (2009).

[18] Noda I, Miyaji F, Ando Y, Miyamoto H, Shimazaki T, Yonekura Y, Miyazaki M, Mawatari M, Hotokebuchi T, "Development of novel thermal sprayed antibacterial coating and evaluation of release properties of silver ions", J. Biomed. Mater. Res. B Appl. Biomater., 89, 456–465 (2009).

[19] Berger TJ, Spadaro JA, Chapin SE, Becker RO, "Electrically generated silver ions: Quantitative effects on bacterial and mammaliancells", Antimicrob. Agents Chemother., 9:357–358 (1976).

[20] Grier N, "Silver and its compounds. In: Block SS, editor. Disinfection, Sterilisation and Preservations. Philadelphia: Lea Febinger; 1983. pp 375–389.

[21] Clement JL, Jarrett PS, "Antibacterial silver", Met. Based Drugs, 1, 467–482 (1994).

[22]Feng QL, Wu J, Chen GQ, Cui FZ, Kim TN, Kim JO, "A mechanistic study of the antibacterial effect of silver ions on Escherichia coli and Staphylococcus aureus", J. Biomed. Mater. Res. A, 52, 662–668 (2000).

[23] Creighton JA, Blatchford CG, Albrecht MG, "Plasma resonance enhancement of Raman scattering by pyridine adsorbed on silver or gold sol particles of size comparable to the excitation wavelength", J. Chem. Soc. Faraday Trans. II, 75, 790–798 (1979).

[24] Lee PC, Meisel D, "Adsorption and surface-enhanced Raman of dyes on silver and gold sols", J. Phys. Chem., 86, 3391–3395 (1982).

[25] Huang HH, Ni XP, Loy GL, Chew CH, Tan KL, Loh FC, Deng JF, Xu GQ, "Photochemical formation of silver nanoparticles in poly(Nvinylpyrrolidone)", Langmuir, 12, 909–912 (1996).

[26] Abid JP, Wark AW, Brevet PF, Girault HH, "Preparation of silver nanoparticles in solution from a silver salt by laser irradiation", Chem. Commun. 7, 792–793 (2002).

[27] De G, Tapfer L, Catalano M, Battaglin G, Gonella F, Mazzoldi P, Haglund RF Jr' "Formation of copper and silver nanometer dimension clusters in silica by the sol–gel process", Appl. Phys. Lett., 68, 3820–3822 (1996).

[28] Mennig M, Schmitt M, Schmidt H, "Synthesis of Ag-colloids in sol–gel derived SiO_2-coatings on glass", J. Sol-Gel Sci. Technol., 8, 1035–1042 (1997).

[29] Carpenter JP, Lukehart CM, Milne SB, Henderson DO, Mu R, Stock SR, "Formation of crystalline nanoclusters of Ag, Cu, Os, Pd, Pt, Re, or Ru in a silica xerogel matrix from single-source molecular precursors", Chem. Mater., 9, 3164–3170 (1997).

[30] Kokkoris M, Trapalis CC, Kossionides S, Vlastou R, Nsouli B, Grotzschel R, Spartalis S, Kordas G, Paradellis, "The RBS and HIRBS studies of nanostructured $AgSiO_2$ sol–gel thin coatings", Nucl Instrum Methods B 2002;188:67–72.

[31] Kreibig U, Vollmer M. Optical Properties of Metal Clusters, Single Clusters: Intrinsic Size Effects of the Optical Properties. Berlin: Springer; 1995. pp 78–118.

[32] Arnold GW, Borders JA, "Aggregation and migration of ionimplanted silver in lithia-alumina-silica glass", J. Appl. Phys. 48, 1488–1496 (1977).

[33] Lee K-C, Lin S-J, Lin C-H, Tsai C-S, Lu Y-J, "Size effect of Ag nanoparticles on surface plasmon resonance", Surf. Coat. Technol. 202,5339–534 (2008).

[34]Ahmed AA, Allah EWA, "Origin of absorption-bands observed in the spectra of silver ion-exchanged soda-lime–silica glass, "J. Am. Ceram. Soc. 78, 2777–2784 (1995).

[35] De G, Licciulli A, Massaro C, Tapfer L, Catalano M, Battaglin G, Meneghini C, Mazzoldi P. Silver nanocrystals in silica by sol–gel processing, J. Non-Cryst. Solids 194, 225–234 (1994).

[36] Ameen KB, Rajasekharan T, Rajasekharan MV, "4Grain size dependence of physico-optical properties of nanometallic silver in silica aerogel matrix", J. Non-Cryst. Solids 352, 737–746 (2006).

[37] Hinsch A, Zastrow A, "The production of small colloidal silver particles in thin SiO_2 sol–gel glass layers", J. Non-Cryst. Solids,147, 579–581 (1992).

[38] Allen LH, Matijevic E. Stability of colloidal silica: III. Effect of hydrolyzable cations. J Colloid Interface Sci 35:66–76 (1971).

[39] Bansal NP, "Influence of several metal-ions on the gelation activationenergy of silicon tetraethoxide," J. Am. Ceram. Soc., 73, 2647–2652 (1990).

[40] Kim YH, Lee DK, Cha HG, Kim CW, Kang YS, Synthesis and characterization of antibacterial Ag–SiO_2 nanocomposite", J Phys. Chem. C, 111, 3629–3635 (2007).

[41] Wu PW, Dunn B, Doan V, Schwartz BJ, Yablonovitch E, Yamane M, "Controlling the spontaneous precipitation of silver nanoparticles in sol–gel materials", J. Sol-Gel Sci. Technol., 19:249–252 (2000).

[42] Kelly KL, Coronado E, Zhao LL, Schatz GC, "The optical properties of metal nanoparticles: The influence of size, shape, and dielectric environment", J. Phys. Chem. B, 107, 668–677 (2003).

[43] Link S, El-Sayed MA, "Shape and size dependence of radiative, non-radiative and photothermal properties of gold nanocrystals", Int. Rev. Phys. Chem., 19,409–453 (2000).

[44] Geng J, Bi Y, Lu G, "Morphology-dependent activity of silver nanostructures towards the electro-oxidation of formaldehyde", Electrochem. Commun., 1,1255–1258.

[45] Kreibig U, Fragstein CV, "Limitation of electron mean free path in small silver particles", Z. Phys. 224:307–323 (1969).

[46] Tanahashi I, Yoshida M, Manabe Y, Tohda T, "Effects of heat treatment on Ag particle growth and optical properties in Ag/SiO_2 glass composite thin films", J. Mater. Res., 10, 362–365 (1965).

[47] Epifani M, Giannini C, Tapfer L, Vasanelli L, "Sol–gel synthesis and characterization of Ag and Au nanoparticles in SiO_2, TiO_2, and ZrO_2 thin films", J. Am. Ceram .Soc., 83, 2385–2393 (2000).

[48] Raffi M, Akhter JI, Hasan MM, "Effect of annealing temperature on Ag nano-composite synthesized by sol–gel. Mater Chem Phys, 99:405–409 (2005).

[49] Ritzer B, Villegas MA, Fernandez Navarro JM, "Influence of temperature and time on the stability of silver in silica sol–gel glasses", J. Sol.-Gel, Sci. Technol. 8:917–921 (1997).

[50] Mennig M, Endres K, Schmitt M, Schmidt H, "Colored coatings on eye glass lenses by noble metal colloids", J. Non-Cryst. Solids, 218, 373–379 (1997).

[51] Kirsi Y, Petra E, Patrick K, Kyo¨ sti K, Guido G. Chemical composition and barrier properties of Ag nanoparticle-containing sol–gel films in oxidizing and reducing low-temperature plasmas", Surf. Coat.Technol., 201:7865–7872 (2007).

[52] Bi HJ, Cai WP, Zhang LD, Martin D, Trager F, "Annealing-induced reversible change in optical absorption of Ag nanoparticles", Appl. Phys. Lett., 81, 5222–5224 (2002)

[53] Li W, Seal S, Megan E, Ramsdell J, Scammon K, Lelong G, Lachal L, Richardson KA, "Physical and optical properties of sol–gel nanosilver doped silica film on glass substrate as a function of heattreatment temperature, J. Appl Phys. 93:9553–9561 (2003).

[54] Akhavan O, Ghaderi E., "Bactericidal effects of Ag nanoparticles immobilized on surface of SiO_2 thin film with high concentration", Curr. Appl, Phys., 9, 1381–1385 (2009).

[55] Hammond JS, Gaarenstroom SW, Winograd N, "X-ray photoelectron spectroscopic studies of cadmium- and silver-oxygen surfaces", Anal. Chem.,47, 2193–2199 (1975).

[56] Hoflund GB, Hazos ZF, Salaita GN, "Surface characterization study of Ag, AgO, and Ag2O using X-ray photoelectron spectroscopy and electron energy-loss spectroscopy", Phys. Rev. B, 62,11126–11133 (2000).

[57] Sakka S, Kozuka H., Sol–gel preparation of coating films containing noble metal colloids. J Sol-Gel Sci Technol 13, 701–705 (1998).

[58] Messerschmidt B, Mclntyre ML, Houde-Walter SN, Andre RR, Hsieb CH, "Temperature dependence of silver-sodium interdiffusion in micro-optic glasses", Opt .Mater., 7, 165–171 (1997)

[59] Garcia MA, Garcia-Heras M, Cano E, Bastidas JM, Villegas MA, Montero E, Llopis J, Sada C, De Marchi G, Battaglin G, Mazzoldi P., Photoluminescence of silver in glassy matrices. J. Appl. Phys., 96, 3737–3741 (2004)

CHAPTER 4

CONCLUSIONS and FUTURE WORK

4.1 Conclusions

4.1.1 Sol-gel processing of silver-doped silica powders

As a general conclusion, the synthesis method significantly affected both the physical and chemical state of silica matrix and the size of metallic silver. One-step acid gelation route leads to formation of dense silica matrix, with a pore size of less than 25 Å. Two-step acid/base catalyzed gelation route, on the other hand, exhibit relatively more open microstructure with bigger pores (250 Å), as revealed by BET analysis. The change in microstructure with synthesis route is related to the pH effect on microstructure for silica gels synthesized from silicon alkoxides.

Another effect of synthesis route is on size and distribution of silver nanoparticles after calcination at 800°C. In acid/base catalyzed silica systems, bigger silver nanoparticles/agglomerates were formed in silica matrix after calcination at 800°C, compared to those formed in acid catalyzed silica gels. The possible reason for the formation of larger silver nanoparticles in acid/base catalyzed silica systems is based on higher probability of precipitation of bigger silver agglomerates in mesopororous silica during gelation and improved diffusion of silver through larger pores of the silica matrix during subsequent calcination.

The synthesis method also affects the size distribution of silver nanoparticles. In acid catalyzed system, the average silver particle size was found similar in the temperature range of 200-800°C; it has a representative homogenous silver particle size of at around 24–30 nm. In acid/base catalyzed silica systems, on the other hand, silver particle size significantly changed with calcination temperature; at lower temperatures at around 400°C silver is distributed in the silica matrix mostly as dispersed nanoparticles and limited agglomerates of silver colloids with an average size of 19 ± 2 nm yet reach 32 ± 2 nm after a heat treatment of 800°C. It has been thought that by an increase in calcination temperature, the number of dispersed colloids decreases and some disappear at the expense of the growth of big agglomerates. This special arrangement of relatively larger silver particles (1) provides a higher potential for silica crystallization through acting as an individual crystallization centers, and (2) improves the final antibacterial percformance.

4.1.2 Sol-gel processing of silver-doped silica coatings

Critical processing parameters to obtain silver doped silica thin films were established. Better surface coverage was obtained by applying multiple coatings. Warm air blowing treatment at 70°C between coating steps provided formation of crack free and homogenous film. Additionally, calcination treatment at moderate tempeartures was found essential to obtain structurally dense film.

The effect of calcination treatment on size and chemical state of silver nanoparticles were investigated. It was observed that silver nanoparticles were mainly in the metallic state in as-prepared condition and after calcination at temperatures lower than 300°C. Silver particles were found exhibiting size variation at lower temperatures; the atomic silver clusters and relatively bigger silver nanoparticles accumulated near the surface. The color of silver containing silica coatings is a light yellowish color, which is indicative for metallic silver. Increasing calcination temperature to 500°C results in oxidation of small silver clusters. This is revealed by thermochromic effect, where the yellow color vanishes after calcination at 500°C. Further increase in temperature to

700°C leads to subsequent reduction of silver oxide to metallic silver, as revealed by reversible dark yellowish color.

Calcination at temperatures higher than 300°C also initiates diffusion of silver from the surface into the bulk of the coating by ion-exchange between silver ions from coating and sodium and calcium ions from glass substrate. The change in surface concentration and distribution of the silver by interdiffusion of sodium and calcium from the underlying glass leads to a degradation in the antibacterial activity.

4.2 Future directions

Previous work indicated that silver particles accumulated on the surface diffused into glass upon thermal treatment at temperatures higher than 500°C, which in turn leads to degredation of antibacterial property. Therefore, it is interesting to consider how the interdiffusion between silver and alkaline glass componenets, such as sodium and calcium is prevented. One possible method to hinder migration of silver particle is deposition of dense SiO_2 interlayer between the glass substrate and the coating. Dense silica layer may prevent ion exchange process between the glass and the coating Furthermore, the silica layer increases the wettability and decreases the difference in thermal expansion coefficient between coating and glass substrate, leading to formation of homogenous, continuous, crack-free, and dense films. This chemical modification can be easily adapated to the processing route, which already explained in this thesis. The use of silica barrier layer between Ag-SiO_2 coating and the substrate might enable use of higher calcination temperature for improved densification and consequently higher chemical durability for the coatings.

Another problem that needs to be solved to improe the lifetime of antibacterial material is associated to chemical durability. When the Ag-SiO_2 coating is exposed to moisture for a long time, silver particles near the surface are easily degraded. In order to alleviate this problem, highly polymerized Ag containing silica network should be developed through modification of silica network with aluminum ions. One can expect that

addition of Al to Ag-SiO_2 films leads to polymerization of silica network due to binding between Ag^+ ions and $[AlO_4]^{--}$ sites, which allows controlled release of silver ions and thus high antibacterial activity. This also eliminates need for high calcination temperatures to obtain dense films, which adversely affecting the chemical composition of silver. Additionally, Al^+ incorporation is useful in obtaining colorless powders.

TEZ FOTOKOPİSİ İZİN FORMU

ENSTİTÜ

Fen Bilimleri Enstitüsü	[X]
Sosyal Bilimler Enstitüsü	[ ]
Uygulamalı Matematik Enstitüsü	[ ]
Enformatik Enstitüsü	[ ]
Deniz Bilimleri Enstitüsü	[ ]

YAZARIN

Soyadı : Akköprü-Akgün
Adı : Betül
Bölümü : Metalurji ve Malzeme Mühendisliği

TEZİN ADI (İngilizce) : Sol-gel processing of silver-doped silica and assesment of its structural and antimicrobial properties

TEZİN TÜRÜ : Yüksek Lisans [X] Doktora [ ]

1. Tezimin tamamından kaynak gösterilmek şartıyla fotokopi alınabilir. [ ]
2. Tezimin içindekiler sayfası, özet, indeks sayfalarından ve/veya bir bölümünden kaynak gösterilmek şartıyla fotokopi alınabilir. [X]
3. Tezimden bir bir (1) yıl süreyle fotokopi alınamaz. [ ]

TEZİN KÜTÜPHANEYE TESLİM TARİHİ: